Electronic Effects in the Electric Double Layer

Wolfgang Schmickler

University of Ulm, D-89069 Ulm, Germany

Received May 17, 1996 (Revised Manuscript Received August 28, 1996)

Contents

Wolfgang Schmickler was born in Bonn, Germany, in 1946. He studied physics and chemistry at the Universities of Bonn and Heidelberg and at the Imperial College, London. In 1973 he received his Ph.D. in Physical Chemistry from the University of Bonn, graduating summa cum laude. His thesis, which was directed by Professor W. Vielstich, was on the theory of electrochemical electron transfer reactions. After completing his degree he received first a Liebig Fellowship of the Verband der Chemischen Industrie and then a Heisenberg Fellowship of the Deutsche Forschungsgemeinschaft. During this time his home university was at Düsseldorf, but he used the freedom that these fellowships offered for visits at the Frumkin Institute of Moscow, the Laboratoire d'Electrochimie Interfaciale du CNRS in Meudon, France, and the IBM Research Laboratory in San Jose. While he was in Moscow he became interested in the theory of the electric double layer; for his work on this subject he received the Bodenstein Award of the Deutsche Bunsengesellschaft in 1985. He became assistant professor at the University of Bonn in the same year, but moved to the United States in 1990, where he held the position of an associate professor at the Utah State University in Logan. In 1992, he returned to Germany and took a faculty position at the University of Ulm, where he has been since. His research interests lie in theoretical electrochemistry, but his group also performs experiments on systems that are of interest to theory.

1. Introduction

All electrochemical reactions take place at the interface between an electronic conductor, the *electrode*, and an ionic conductor, the *electrolyte*. Since the course of these reactions and their variation with the electrode potential depend on the distribution of the particles and the charges in this interfacial region, its structure is of paramount importance for electrochemistry and has been a topic of intensive research since the time of Lippmann[1] and Helmholtz.[2] It was Helmholtz who pointed out that the high capacity of the interface between a metal and a concentrated electrolyte solution could be explained by the existence of two layers of charges of equal magnitude and opposite sign: a layer of charge on the metal surface, which is balanced by an ionic excess charge in the adjacent solution. This distribution of charges became known as the *electric double layer*; the use of this term is generally restricted to metal electrodes, and so is this review.

Figure 1 shows a picture of the double layer between a single-crystal metal electrode and an aqueous electrolyte solution; this is the interface that is studied in most of the works on which we will report. The circles on the left denote the ion cores of the metal. The polar solvent molecules are indicated by circles with an arrow at their center, and the ions

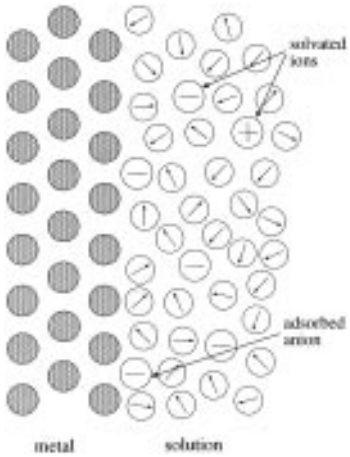

Figure 1. Schematic picture of the double layer between a metal surface and an electrolyte solution.

S0009-2665(94)00408-5 CCC: $25.00

are represented by circles with charges. The metal is assumed to carry an excess positive charge (which is not shown) located at the surface, which is compensated by an excess of anions on the solution side of the interface. Several anions are specifically adsorbed and, hence, in contact with the metal, while others are separated from the metal by solvent molecules. Double layer studies try to obtain information on the actual distribution of the particles and the charges, which is shown schematically here.

The development of microscopic models for the double layer began with the works of Gouy[3] and Chapman,[4] who proposed a space charge theory for the solution part of the double layer. Their theory explains the interfacial capacity at low (i.e., less than about 10^{-3} M) electrolyte concentrations quantitatively. This success induced researchers to focus on the structure of the solution at the interface, while the metal continued to be treated as a perfect conductor, whose electronic properties were disregarded. The period until about 1980 was marked by the development of quite detailed models for the distribution of ions and solvent molecules, but quantitative agreement with experimental data for the interfacial capacity could only be achieved by fitting a fair number of adjustable parameters. The strong effect of the metal on the interfacial properties, which is evident from the capacity−charge characteristics discussed in section 2, could not be explained by these models.[5]

A notable exception to this single-minded focus on the solvent structure was the early work of Rice.[6] He was the first to consider the spatial distribution of the electronic charge on the metal surface in the context of double layer theory. Using the Thomas−Fermi model he calculated the penetration of the electric field into the metal surface and pointed out that the metal itself should make a contribution to the interfacial capacity. Unfortunately, the Thomas−Fermi theory is not well suited to describe the properties of metal surfaces—indeed, it predicts that the work function of any metal should be zero. It is therefore not surprising that the work of Rice predicts values for the interfacial capacity that are far too small and essentially independent of the metal. For these reasons his work was forgotten for several decades.

Until about 1980 experimental electrochemistry was mainly restricted to measurements of potential and current, which give little information on the interfacial structure. At about that time techniques became available that can probe the electronic properties of the metal surface directly. Simultaneously, theoreticians began to reconsider the distribution of the electrons on the metal surface using the *jellium* model, which is much better at describing surface properties than the Thomas−Fermi theory. The first applications of the jellium model offered immediately a qualitative explanation why the double layer capacity depends so strongly on the nature of the metal. This first success spurned considerable theoretical activity, and the development of double layer models by various groups of researchers. While these models differ in details, they agree on the basic mechanism by which the surface electrons influence

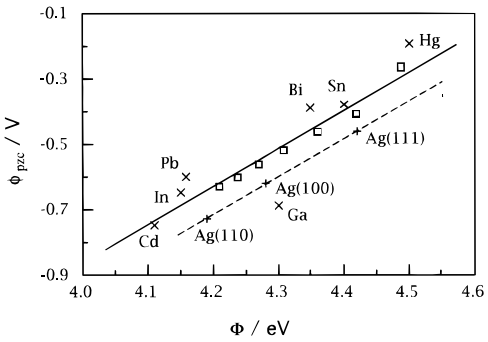

Figure 2. Potential of zero charge of several groups of metals versus their work function. The sp metals are indicated by ×, the work functions of the solid metals are for polycrystalline samples; data were taken from Trasatti.[7] The indium amalgams are indicated by □; these data are from ref 11. The solid line indicates the correlation for the sp metal including the amalgams; the dashed line is for the silver surfaces.

the double layer capacity. In addition, they offer a framework in which the electronic effects evidenced by new techiques, such as second harmonic generation or electroreflectance, can be understood.

We will begin this review by looking at a few phenomenological correlations that clearly demonstrate the effect of the electronic properties of the metal on the double layer. Thereafter, we will outline the jellium model and its extensions, which form the basis of much of our present understanding of these effects. Then, we will review a number of modern techniques that actually probe the electronic surface structure, and provide illustrative examples. But electronic effects manifest themselves not only in the structure of the interface but also in electron transfer, in the reactions of hot electrons, or in electron tunneling through the double layer. Those topics will covered before we finally discuss attempts to construct complete models for the double layer.

2. Phenomenological Correlations

2.1. The Potential of Zero Charge

A metal electrode carries a charge density whose magnitude depends on its potential. The unique potential ϕ_{pzc} at which it carries no charge is called the *potential of zero charge* (pzc). It is a characteristic quantity for a particular metal/solvent interface and independent of the ions, provided there is no specific adsorption. It is found to correlate with its work function Φ in the following form

$$\phi_{pzc} = \Phi + C \qquad (1)$$

where the constant C depends on the scale on which the electrode potential is measured; for the standard hydrogen electrode (SHE) its value is approximately 4.5 eV. The correlation is somewhat rough; it becomes better if the metals are grouped into various chemical classes: the sp, the sd (Cu, Ag, Au), and the transition metals. Figure 2 shows the data for polycrystalline sp metals, a few surfaces of single crystal silver electrodes, and a series of indium amalgams. We have left out the transition metals because there are only few data for single crystals,

but we note that the values for polycrystalline metals do follow eq 1.[7]

This correlation is easily derived from a thermodynamic cycle, in which the electron is transferred from the metal first into the vacuum, then into the solution, and then back to the metal; the details can be found in the literature.[7,8] As a result, the potential of zero charge can be expressed through the work function of the metal (labeled M) and the difference in the outer potential between the metal and the solution (labelled sol). (A brief reminder: the inner potential ϕ is the electrostatic potential *inside* a phase, the outer potential ψ is the potential just *outside* the phase. They differ by the surface potential $\chi = \phi - \psi$, which is caused by an inhomogeneous charge distribution at the surface. In polar liquids the surface potential is due to a small net orientation of the dipole moments at the surface; in metals it is caused by the different distribution of the ionic and the electronic charges. These points are discussed at greater lengths in section 3.) On the standard hydrogen scale

$$\phi_{pzc} = (\Phi_M - \Phi_{ref})/e_0 + (\psi_M - \psi_{sol}) \qquad (2)$$

where Φ_{ref} is the work function of the hydrogen evolution reaction under standard conditions, which is defined as the work required to transfer an electron from a hydrogen molecule in the solution to a position in the vacuum just outside the solution by the process:

$$1/2\ H_2(\text{solution}) \rightarrow H^+(\text{solution}) + e^-(\text{vacuum})$$

The exact value of this work function, which links the electrochemical scale of potentials to the vacuum scale, has been the subject of some debate.[9] Due to the uncertainty in the experimental quantities that enter into its definition, it can presently be given only with a substantial uncertainty: $\Phi_{ref} = (4.5 \pm 0.2)$ eV.

Equation 2 already suggests a correlation of the pzc with the work function. The last term, which has the meaning of a contact potential, does not vanish at the pzc, because the dipole potentials of the solvent and of the metal change when they are brought into contact: the interaction of the solvent with the metal surface modifies the net orientation of the solvent molecules. For example, water molecules tend to be oriented with their oxygen end toward the metal, and the electronic density of the metal is modified through the interaction with the water. Denoting these changes in the dipole potentials by $\delta\chi_{sol}$ and $\delta\chi_M$ we obtain finally:

$$\phi_{pzc} = \frac{1}{e_0}(\Phi_M - \Phi_{ref}) + \delta\chi_M - \delta\chi_{sol} \qquad (3)$$

The work function of the reference electrode is a constant, and the dipole potential terms are small. Therefore, the work function of the metal is the dominant term on the right hand side, which explains the observed correlation. The constant C in eq 1 should be close to the work function of the reference electrode, which is indeed the case. The small deviations from this correlation that are observed, and the grouping into different classes, are caused by the dipole terms and can be used to obtain the changes in the dipole potential on the formation of the interface. Thus, this correlation can be understood without recourse to a microscopic model. It does not hold when the solution contains ions that are specifically adsorbed, because adsorption changes the dipole potential at the interface in the same way that it changes the work function of a metal surface in the vacuum.

Metal work functions correlate with several other quantities, in particular with the density of surface atoms or, equivalently, the density of broken bonds on the surface. Therefore, the potential of zero charge correlates with these quantities as well.[10]

2.2. The Helmholtz Capacity

For a long time the models of the electric double layer were based on the interfacial capacity, which can be obtained with relative ease from measurements of currents, potentials, and in the case of liquid electrodes, the surface tension. The first quantitative theory was that of Gouy and Chapman; it is equivalent to the Debye−Hückel theory, which it predates by more than a decade. Just like the latter, it models the solution as an ensemble of point ions in a dielectric continuum, while the metal is treated as a perfect conductor. It is valid in the limit of low electrolyte concentrations—for a 1−1 electrolyte up to about 10^{-3} M—and gives the following explicit formula for the differential capacity per unit area

$$C = \frac{\partial\sigma}{\partial\phi} = \frac{\epsilon\epsilon_0}{L_D}\cosh\left(\frac{ze_0(\phi - \phi_{pzc})}{2kT}\right) \qquad (4)$$

where σ is the surface charge density, L_D the Debye length, and ϵ the dielectric constant of the solvent. Obviously, the Gouy−Chapman capacity contains no information on the microscopic structure of the interface. It has a pronounced minimum at the potential of zero charge, from which the latter can be determined.

At higher concentrations systematic deviations from the Gouy−Chapman theory are observed. If there is no specific adsorption of ions the interfacial capacity is found to obey the relation

$$\frac{1}{C} = \frac{1}{C_{GC}} + \frac{1}{C_H} \qquad (5)$$

where C_{GC} is the Gouy−Chapman capacity from eq 4 and C_H is called the *Helmholtz capacity* (it is also known as the *inner layer* or the *compact layer* capacity). The Helmholtz capacity is independent of the electrolyte concentration and varies only weakly with the nature of the ions. In practice, there is almost always some specific adsorption of anions at potentials above the pzc, which may lead to deviations from eq 5.

The Helmholtz capacity can be determined by measuring the capacity C at various electrolyte concentrations and plotting $1/C$ versus the inverse of the calculated Gouy−Chapman capacity (*Parsons and Zobel* plot[12]). In practice, the Helmholtz capacity is close to the capacity measured at concentrations

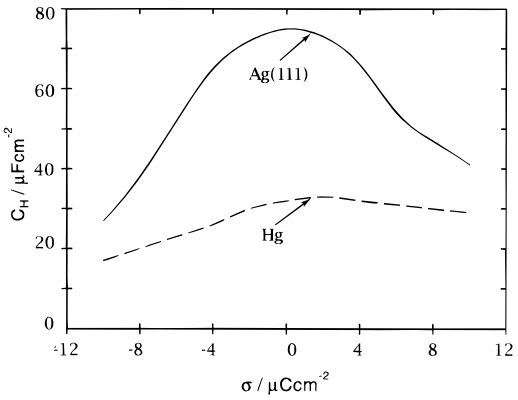

Figure 3. Helmholtz capacity as a function of the electrode charge for mercury and Ag(111) in contact with an aqueous solution of ions that are not specifically adsorbed.

of about 1 M since at such concentrations the Gouy–Chapman capacity is large and its inverse small.

The Helmholtz capacity depends on the charge density on the electrode; Figure 3 shows two such capacity–charge characteristics. They depend strongly on the nature of the metal and of the solvent and thus contain the information on the microscopic structure of the interface that is missing in the Gouy–Chapman part. Explicit models will be discussed below; here we will briefly indicate the origins of the Helmholtz capacity, which resides in a number of effects that are not considered in the Gouy–Chapman theory:

(1) Near the interface the solution possesses a definite structure, which manifests itself as oscillations in the particle density, which in turn gives rise to oscillations in the potential.

(2) At high electrolyte concentrations the Debye length, and hence the spatial extension of the double layer, is short. Therefore, the electric field can reach extremely high values, of the order of 10^9 V m^{-1}. This leads to dielectric saturation in the layers of solvent molecules at the interface.

(3) This high field strength distorts the electronic density at the metal surface so that the surface potential of the metal is changed. This effect is one of the main topics of this review.

It was first noted by Trasatti[7] that the Helmholtz capacities of the simple sp metals, taken at the pzc, correlate with their electronic densities (see Figure 4). There is some scattering of the data, but overall the trend seems to hold in those solvents for which data exist. This correlation illustrates the important role played by the response of the surface electrons to the electric field. Its origin will be discussed in the next section.

3. The Electronic Density at a Metal Surface

The preceding discussion has shown that the electronic structure of the metal surface has a profound infuence upon the double layer properties. This may sound trivial, but for a long time the metal surface was regarded as a structureless perfect conductor, and the role of the surface electrons was only recognized recently.

Double layer theory is a very active area of research. At the present time there is broad agreement

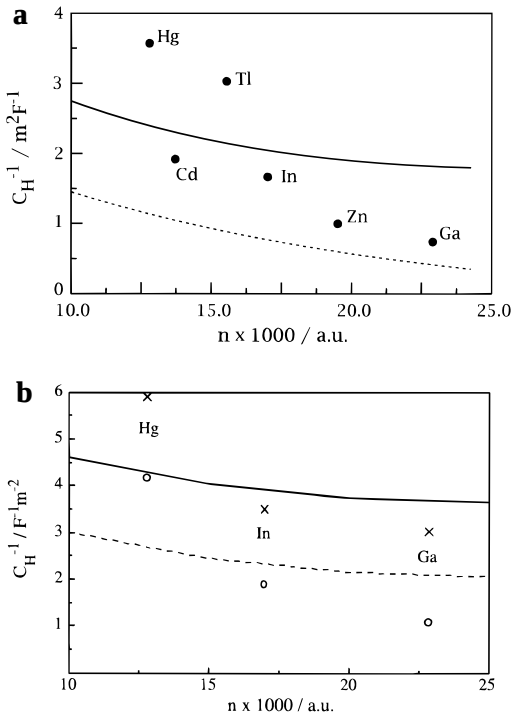

Figure 4. Helmholtz capacity at the pzc for simple sp metals: (a) aqueous solutions; (b) crosses (×) and full line demethyl sulfoxide; circles (○) and dashed line, acetonitrile. The lines are explained in section 9.1. The electronic density is given in atomic units (au); 1 au of density corresponds to 6.75 × 10^{24} cm^{-3}.

on the type of models that should be used for the metal and for the solution, and a number of qualitative effects seem to be established. The most difficult problem is the interaction of the metal surface with the solution. In this point the models that have been put forward by various groups differ considerably; all of them are relatively simple, and a fully self-consistent treatment is still lacking.

In this section we present models for the electronic structure of the electrode; complete double layer models, which include also the solvent, will be discussed in section 9.

3.1. The Jellium Model

The biggest recent advance in double layer theory was the introduction of the jellium model.[13,14] Before this model was used in electrochemistry, it had been used extensively in the theory of metal surfaces.[15,16]

A metal consists of electrons and a lattice of positively charged ions. In the jellium model the ionic charge is represented by a constant positive background charge, which drops abruptly to zero at the metal surface, whose position is also denoted as the *jellium edge*. The electrons are modeled as an inhomogeneous electron gas, which interacts with the positive background. The quantum-mechanical self-interactions of the electron gas—the exchange and the correlation energies—are treated in the *local density approximation*, which is based on the following idea: these interactions are well known for an electron gas of constant electronic density. To a first approximation one can assume that in an inhomogeneous gas the exchange and correlation energies at each point take on the same values that they

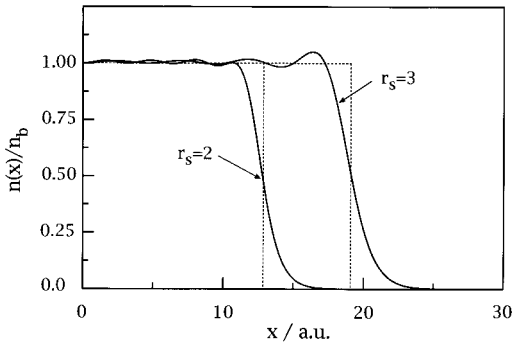

Figure 5. Electronic density profile at the surface of *jellium* for two different bulk densities. The positive background charge is indicated by the dashed line. For clarity, the jellium edge was taken at different positions for the two cases. Note: 1 au of distance is 0.529 Å.

would have in a homogeneous gas with the same density. While this approximation is simple, it has the advantage that it fulfills a number of sum rules which the exact expression must also obey. Most importantly, it gives good results for the electronic structures of surfaces, and only for complicated interactions one has to resort to better mathematical treatments like the generalized gradient approximation.

Explicit calculations for the electronic density profile of jellium are based on the *density functional formalism* developed by Hohenberg, Kohn, and Sham.[17] Both exact[16] and good approximate treatments[15,18] are available. In the jellium model the properties of a metal surface are completely determined by the bulk electronic density n_b or, equivalently, by the *Wigner−Seitz* radius r_s, which is the radius of a sphere containing one electron, i.e., $n_b = 3/4\pi r_s^3$. Figure 5 shows the electronic density profiles for two different values of r_s. The most important feature is the relatively slow decay of the electronic density at the surface, which occurs over a distance of 1−2 Å and is caused by the small electronic mass; this effect is also known as the *electronic spillover* at the surface. On the metal side of the surface the density profile exhibits small oscillations, the *Friedel oscillations*,[19] which are more pronounced for lower bulk densities.

The slow decay of the electronic density profile entails a small but appreciable negative charge density on the outside of the surface, which for an uncharged surface is balanced by a positive excess charge on the inside. This charge distribution gives rise to a dipole moment and a surface dipole potential of the order of a few volts—this is precisely the dipole potential χ_M discussed in the preceding section. Since the dipole moment is directed with its positive end toward the bulk, an electron leaving the metal must perform work against the dipole potential, which therefore makes an important contribution to the work function. The total work function is given by $\Phi = -\mu_b + e_0\chi$, where μ_b is the chemical potential of the electrons in the bulk, which in the jellium model is caused by the exchange and correlation interactions of the electrons.

Obviously, jellium is a conceptually simple model for a metal, even though explicit calculations within this model are not easy. It does not account for

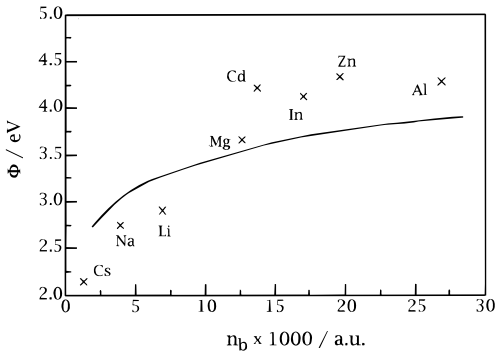

Figure 6. Work function of selected polycrystalline sp metals as a function of their electronic density; the line indicates the prediction of the jellium model.

lattice structure and cannot describe d bands, which are narrow and more localized than the sp bands. Its application is therefore limited to polycrystalline sp metals; modified versions have also been applied to the sd metals Cu and Ag; they will be discussed in the next subsection.

In the jellium model the properties of a metal are solely determined by its electronic density. Figure 6 shows the theoretical curve for the work function Φ versus the bulk electronic density n_b, together with experimental data for polycrystalline sp metals. The theory explains the increase of the work function with the electronic density and gives the correct order of magnitude. While large-scale quantum-chemical calculations reproduce work functions with a greater accuracy than the jellium model, they add little to our understanding.

We note in passing that the Thomas−Fermi model does not contain the effects of the electronic spillover. This is one of the reasons why it fails to explain phenomena such as the work functions of metals and the double layer capacity.

For double layer theory the important quantity is not the work function itself but the surface dipole potential, which figures not only in eq 3 for the potential of zero charge but also in the interfacial capacity C. To see this we consider the inverse:

$$\frac{1}{C} = \frac{\partial(\phi_M - \phi_{sol})}{\partial\sigma} \tag{6}$$

Since the surface potential χ_M is a part of the potential difference $(\phi_M - \phi_{sol})$ we can define the metal contribution to the inverse capacity as

$$\frac{1}{C_M} = \frac{\partial\chi_M}{\partial\sigma} \tag{7}$$

so that formally

$$\frac{1}{C} = \frac{1}{C_M} + \frac{1}{C_{sol}} \tag{8}$$

where the last term gives the variation of the remainder of the potential, which is attributed to the solution, with the surface charge density. It is important to realize that the contribution of the metal to the capacity is *negative* since the surface potential decreases when the metal is positively charged. This follows from Le Chatelier's principle: A positive

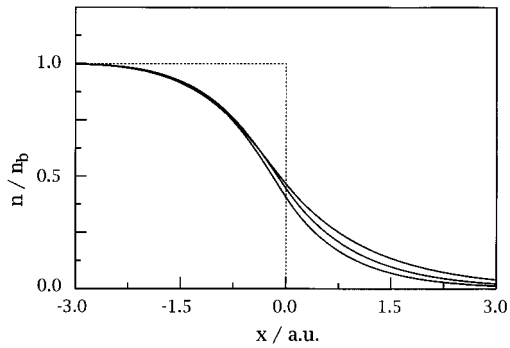

Figure 7. Schematic diagram of the response of the electronic density profile at the surface to an external field. The upper curve is for a negatively charged surface, the lower for a positive charge, and the curve in the middle is for an unchared surface. The positive background charge is indicated by the dashed line.

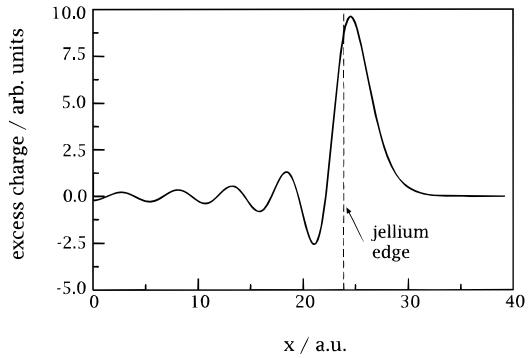

Figure 8. Distribution of a small excess charge on the surface of jellium with a bulk density of 8.9 au, arbitrary units.

charge density increases the potential drop between the metal and the solution, and the surface electrons react so as to make it smaller. Thus, a positive charge density on the metal surface gives rise to an electric field directed outward from the surface, which pulls the electrons back into the metal and thereby decreases the surface dipole moment. Conversely, a negative charge pulls the electrons toward the solution and increases the surface potential (see Figure 7). Since the metal capacity is negative it makes the total capacity, which must be positive in any reasonable model, larger. In essence: the metal surface possesses a high electronic polarizability, which increases the double layer capacity. Since the metal capacity is independent of the concentrations of the ions in the solution, it enters into the Helmholtz capacity.

The metal contribution to the capacity can be related to another quantity: the effective position of the image plane. Since the electrons on the surface of jellium react to the presence of an external field, it does not behave like a perfect classical conductor. A small test charge situated in front of a jellium surface induces a surface charge of equal magnitude and opposite sign. However, this small excess charge is not located right on the metal surface; the major part lies in front of the jellium edge, and there are oscillations in the induced charge density (see Figure 8). As a consequence, the test charge experiences a modified image law, in which the image plane is not situated at the jellium edge, where the positive background charge drops to zero, but a small distance

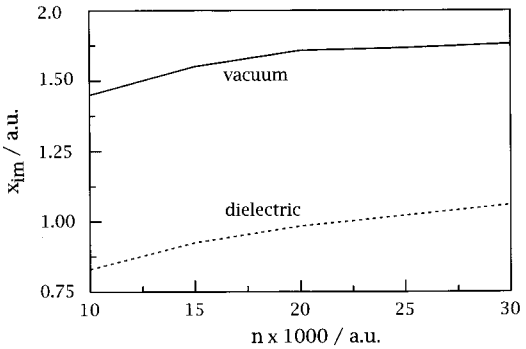

Figure 9. Position of the effective image plane as a function of the bulk electronic density.

x_{im} in front. A simple calculation shows that[20]

$$x_{im} = \frac{\int x\delta\rho(x)\,dx}{\int \delta\rho(x)\,dx} = -\epsilon_0 \frac{\partial\chi}{\partial\sigma} = -\epsilon_0 \frac{1}{C_M} \qquad (9)$$

where $\delta\rho(x)$ is the excess charge density on the metal. Likewise, the capacity of a condenser composed of two identical jellium plates is given by the classical equation, but the effective plate separation is smaller than the physical separation by an amount $2x_{im}$. We will see later that the same quantity plays also an important role in second harmonic generation.

The value of the image plane position x_{im}, calculated for an uncharged metal surface, increases with the electronic density (see Figure 9); this is to be expected, since a higher electronic density should entail a greater polarizability. This immediately explains the tendency of the Helmholtz capacity to increase with the electronic density of the metal, which was observed in Figure 4. For a quantitative comparison one requires an estimate for the contribution C_{sol} of the solution to the inverse capacity. This will be further discussed in section 9.

The interaction of the surface electrons with the solution is a very active and controversial area of research and will be considered in greater detail below. From experiments in the vacuum it is known that water is only weakly adsorbed on sd metals like silver and copper, while it interacts more strongly with the transition metals. There are no data for the sp metals, but since water seems to interact with the d electrons it is probably safe to assume that the interaction of sp metals with water is weak. In the simplest model that has been proposed[21] that part of the electronic density that spills over into the solution is supposed to interact with the electronic polarizability of the solvent molecule; therefore, the region outside the jellium edge is assumed to have the optical dielectric constant ϵ_{opt}, which weakens the electrostatic self-interaction of the electrons and reduces the field. The optical constant is chosen because the correlation lengths of the other two modes that contribute to the static dielectric constant, *viz.* the rotation and the distortion of the solvent molecules, are longer than the distance over which the electrons penetrate into the solvent. This simple assumption leads to a significant decrease of the effective image plane position (see Figure 9).

The position of the effective image plane depends on the surface charge density of the surface (see

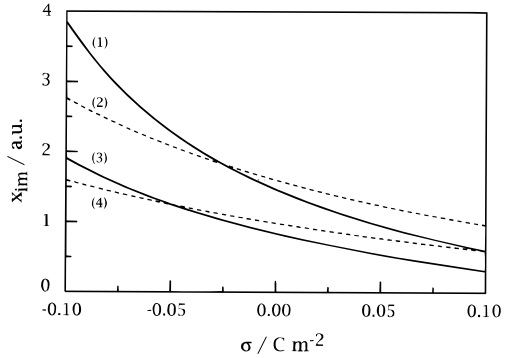

Figure 10. Position of the effective image plane as a function of the surface charge density for jellium in the vacuum and for jellium in contact with a dielectric with $\epsilon_{opt} = 1.88$: (1) $r_s = 3$ (vacuum); (2) $r_s = 2$ (vacuum); (3) $r_s = 3$ (dielectric); (4) $r_s = 2$ (dielectric).

Figure 10). It is higher at negative charge densities, where the electrons spill out further, than at positive charges, where the electrons are withdrawn toward the bulk. Thus, the response to an external charge is nonlinear, which has important consequences on the optical properties; this will be shown in the section on second harmonic generation.

3.2. Jellium with Pseudopotentials

In the simple jellium model the metal is characterized by its electronic density only. While this is sufficient to describe general trends, it does not account for the effect of lattice structure and can therefore not explain the differences between the various surface planes of single crystals. In a popular extension of this model the positive background charge is replaced by a lattice of pseudopotentials (see Figure 11). At each lattice site the electrons are subjected to a potential that at short distances is governed by the electronic repulsion from the core and at large distances by the Coulomb force. Various forms of pseudopotentials have been proposed. The simplest is the Ashcroft form[22]

$$v(r) = \begin{cases} 0 & \text{if } r < r_c \\ -\dfrac{ze_0}{r} & \text{if } r \geq r_c \end{cases} \qquad (10)$$

where z is the charge number of the ion and r_c is the radius of the pseudopotential. In this simple model the electronic repulsion is assumed to cancel the Coulomb attraction inside a sphere of radius r_c. For each metal the value of r_c is chosen such that the model reproduces the bulk properties of the metal (e.g., cohesive energy, bulk modulus) well. Alternatively, r_c can be calculated from the condition that the metal should be stable against changes in density. These prescriptions lead to slightly different recommended values for r_c.

The surface plane of the metal is situated at a distance $d_0/2$ in front of the first lattice plane (see Figure 11), where d_0 is the spacing of the lattice planes in the direction perpendicular to the surface. This choice ensures that for an uncharged metal surface the ionic charge is balanced by the electronic charge.

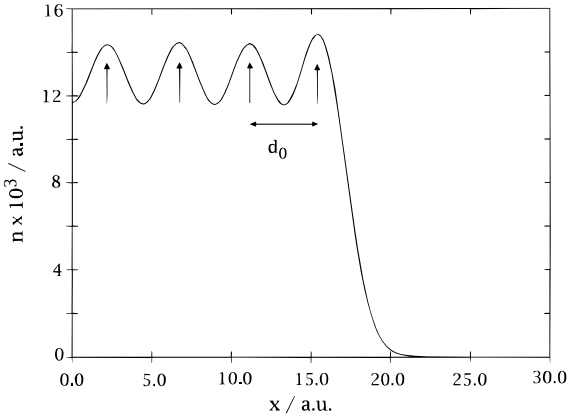

Figure 11. Electronic density profile for jellium with a lattice of pseudopotentials. The positions of the ion cores are indicated by arrows.

To keep the model one-dimensional the pseudopotentials are often averaged in the direction parallel to the metal surface. This procedure gives good results for average properties like the metal work function and the surface energy;[23] it is commonly employed in calculations for electrochemical systems.

This extended jellium model makes it possible to perform calculations for different surfaces of a single crystal. In addition, Russier and Badiali[24] have shown that it can be used to describe the sd metals copper and silver, if the mixing of the d states with the sp band is taken into account by assigning a formal valence of 1.5 to the Cu and Ag ion cores. Their model gives good values for the work functions of the principle surface planes of these two metals; it has also been used for calculations of the electrochemical and optical properties of these surfaces with some success (see below). Copper and silver are among the most important electrode materials, so simple models for these metals are particularly welcome. Unfortunately, the relativistic effects in gold cannot be incorporated into the jellium model so easily, and an extension to transition metals seems impossible.

With the introduction of pseudopotentials the electronic density in the bulk is no longer uniform, but shows maxima in the vicinity of the lattice sites and minima in between the lattice planes (see Figure 11). Near the surface, the decay of the density is similar to that observed in the simple jellium model, but the decay length, and hence the surface dipole moment, depends on the surface plane, so that the work functions are also different. Of considerable interest to electrochemists is the fact that the effective position of the image plane also varies. The corresponding values for the principal planes of silver have been calculated by Leiva.[25] In these calculations the pseudopotentials were averaged in the direction parallel to the metal surface. A proper three-dimensional calculation for Ag(100) by Aers and Inglesfield[28] gave practically the same result (see Table 1). Earlier calculations by Henderson and Schmickler[26] and by Amokrane and Badiali,[27] both based on the variational method, gave the same ordering for the three principle planes, but somewhat different values. A comparison with the experimental data for the Helmholtz capacity[29] shows that this model indeed predicts the correct ordering for these

Table 1. Image Plane Position and Helmholtz Capacity[29] for the Principle Planes of Silver Single Crystals (a) from Ref 25 and (b) from Ref 28 (d_0 Denotes the Spacing of the Lattice Planes)

face	$x_{im}{}^a$/Å	$x_{im}{}^b$/Å	$x_{im} + d_0/2$/Å	C/F m^{-2}
Ag(111)	0.20		1.38	0.69
Ag(100)	0.50	0.51	1.54	0.90
Ag(110)	0.80		1.53	1.08

planes: both the position of the image plane and the Helmholtz capacity increase in the sequence Ag(111) > Ag(100) > Ag(110). However, the position of the image plane varies considerably between the planes, while the differences in the Helmholtz capacities are relatively minor. Therefore, it has been suggested that the position of the interface is not given by the jellium edge, which lies at the face-dependent distance $d_0/2$ from the top lattice plane, but by the radius of the metal atoms. In this case the quantity that determines the metal capacity would be $x_{im} + d_0/2$, which shows less variation (see Table 1). At the time of writing this review, the position of the interface is a matter of debate, and we will return to this question below.

4. Electronic Effects Observed by Optical Techniques

The classical electrochemical techniques measure charge, potential, and current—and in the case of liquid metals the surface tension as well. While the results of such measurements cannot be understood without considering the electronic structure of the interface, they do not give detailed information about it. Quantities like the interfacial capacity depend on the distribution of all the particles, electrons, ions, and solvent molecules. Hence, a quantitative interpretation requires a detailed microscopic model, and several different models may be compatible with the data. Optical techniques that use light in the visible or near-ultraviolet region probe the electronic response to the incoming radiation directly and, hence, may provide information that is lacking in the classical measurements. We will provide examples from two methods: *uv−visible reflectance spectroscopy* and *second harmonic generation*.

4.1. Electroreflectance Spectroscopy

When light is incident on the interface between two media the amount reflected depends on the dielectric properties of the two adjoining phases. Aqueous solutions are transparent to light in the visible and near-ultraviolet region of the spectrum; therefore, the reflection coefficient of the interface between a metal and an aqueous solution, measured as a function of the photon energy, depends mainly on the optical properties of the metal surface. In electroreflectance spectroscopy monochromatic light is incident on an electrode surface, and the reflected light is investigated as a function of the frequency. To enhance the sensitivity, difference spectra are recorded: the reflectivity R of the surface is first measured at a chosen reference potential, then the potential is stepped to some other value, and the differences ΔR between the sets of values are taken. The resulting

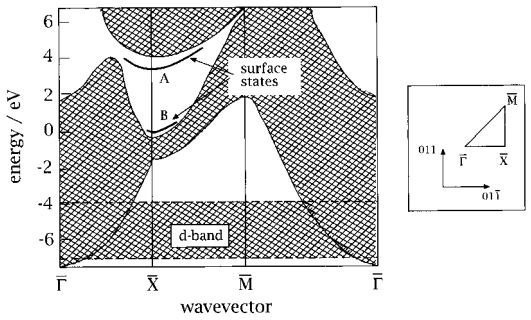

Figure 12. Projected band structure of Ag(100). The energies are given with respect to the Fermi level.

spectra, usually plotted as $\Delta R/R$ vs the photon energy, are known as *electroreflectance spectra*. The use of this technique implies that the optical properties of a metal electrode vary with the potential or, equivalently, the charge density of the metal surface. Indeed, external fields penetrate a few angstroms into the metal surface, and the induced charge density extends over the same distance. Therefore, the electric field on the surface, and the resulting depletion or accumulation of electrons, affects the optical properties.

The dielectric constant $\hat{\epsilon}(w)$ of a metal is a complex quantity and generally contains contributions both from free and from core electrons. Therefore, minor changes in the reflectivity are difficult to interpret, and the method is most useful to detect gross changes in the optical constants. A case in point is the occurence of surface states. Electronic transitions from occupied bulk states to empty surface states decrease the reflectivity at the associated photon energy. Since surface states are localized in the region that is sensitive to external fields, their position relative to the metal Fermi level varies with the applied potential. Hence, transitions to surface states show up as positive or negative peaks in the difference spectra that constitute the electroreflectance signal.

The best studied systems are the surfaces of silver single crystals. We consider the Ag(100) plane in greater detail. Figure 12 shows the projected band structure of this surface as calculated by Ho et al.[30] It exhibits two surface states, labeled *A* and *B*; the latter lies close to the Fermi level, the former several electron volts higher. Transitions from occupied bulk states to these surface states show up as two sets of peaks in the electroreflectance signal (see Figure 13).[31] On the SCE (saturated calomel electrode) scale the potential of zero charge of the Ag(100) electrode lies at −0.9 V. Transitions into the higher state *A* appear at potentials above the hydrogen evolution reaction near the 3 eV region. With increasing electrode potential they shift to higher values, and above −0.6 V they move into the interband transition and disappear. At about the same potential the surface state *B* be has been raised above the Fermi level, and transitions into *B* show up as characteristic dips at lower energies in the electroreflectance spectrum. With increasing electrode potential this surface state is also shifted to higher energies as expected. Simultaneously, its width seems to increase.

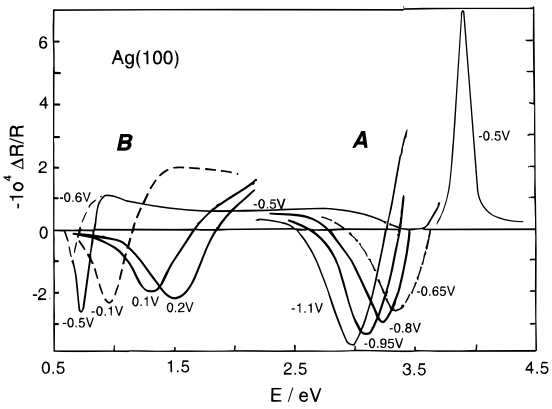

Figure 13. Normal-incidence electroreflectance spectrum of Ag(100) in 0.5 M NaF solution for various bias potentials; *E* denotes the photon energy. Reprinted from Boeck, W.; Kolb, D. M. *Surf. Sci.* **1982**, *118*, 613. Copyright 1982 Elsevier.

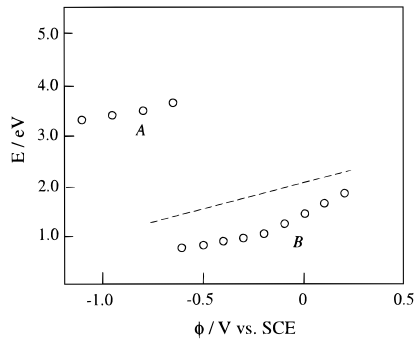

Figure 14. Shift in transition energy with the electrode potential for the two surface states on Ag(100); the dashed line is a guide to the eye and has unit slope. Data taken from ref 30.

These shifts in the position of the peaks with the electrode potential merit closer attention. The surface states are localized at a position about 1 Å in front of the first lattice plane and should therefore experience an electrostatic potential intermediate between those of the two bulk phases. Therefore, we should expect them to shift with a certain fraction of the electrode potential. A quantitative evaluation of the spectrum shows that this is indeed the case for surface state *B* (see Figure 14), while the spectra for state *A* show a stronger shift at higher potentials, where the shift of the energy is even greater than that of the potential. The cause for this behavior is not quite clear. It may be caused by the specific adsorption of anions, which would repel electrons in the surface states, thereby increasing their energy. Alternatively, it could be caused by oscillations in the local electrostatic potential due to the water structure at the interface, an effect that will be discussed further below.

The width of the surface states that appears in the electroreflectance spectra is greater than predicted by the calculations, which were performed for an ideal surface in vacuum. The states are probably broadened by the interaction with the water dipoles, which exhibits thermal fluctuations.

With special experimental arrangements the incident light can excite *surface plasmons*. These are charge density waves of the electron gas that propagate parallel to the surface, while their amplitude

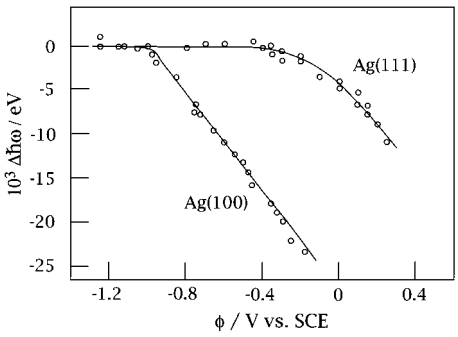

Figure 15. Shift of the surface plasmon frequency with electrode potential; data taken from ref 34.

decays exponentially toward the bulk. On a perfectly flat electrode surface the excitation of surface plasmons is forbidden by momentum conservation. However, surface roughness or, preferentially, an arrangement known as *attenuated total reflectance*,[32,33] in which the evanescent part of the light beam couples to the plasmons, can provide the necessary momentum transfer. This makes it possible to measure the dispersion curves of the plasmons, and, what is more important, their energy as a function of the electrode potential. Figure 15 shows the results for Ag(111) and Ag(100) surfaces.[34] In both cases the plasmon energy is practically constant below the point of zero charge, but decreases noticeably at higher potentials. This phenomenon cannot be explained in terms of the jellium model, since this predicts a plasmon frequency that is practically constant[35]—the changes in the electronic density at the surface are too small to affect the surface plasmon frequency. Possibly this effect is related to the adsorption of anions.

4.2. Second Harmonic Generation

There are several techniques that depend on the nonlinear optical properties of matter. The one that is employed most often in electrochemistry is second harmonic generation (SHG). The principle of this method is quite simple: intense laser light of a certain frequency ν is incident on the metal−solution interface, and the light that emerges at the frequency 2ν is examined. There is an important selection rule: within the electric dipole approximation, substances that are centrosymmetric do not generate second harmonic (SH) light. Since electrolyte solutions and practically all electrode materials possess this symmetry, the observed signal comes mostly from the interface, where the symmetry is broken.

There are various applications of second harmonic generation in electrochemistry; they are reviewed in several excellent articles;[36−38] here, we shall focus on those aspects that give information on the electronic properties of the surface.

The observed signal is usually strongest in the so-called p-in p-out configuration, in which the incident beam is polarized in the p-direction (i.e., its polarization vector has a component perpendicular to the interface), and the signal with the same polarization is observed. For a given system the intensity of the signal depends on both the polar and the azimuthal angle of incidence. The dependence on the polar angle gives important information about the sym-

metry of the surface but tells less about the electronic response. Therefore, we will focus on the signal that has been averaged over the polar angle. On flat metal electrodes there are three sources that give rise to frequency doubling, and the observed signal is caused by their interference. Explicitly we can write

$$I_p^{2\nu} \propto [fa(\nu)E_x^2 + gb(\nu)E_xE_{||} + hd(\nu)\mathbf{E}\cdot\mathbf{E}]^2 \quad (11)$$

where the symbols have the following meaning: **E** is the electric field vector of the incident light, $E_{||}$ its parallel, and E_x its perpendicular component; f, g, h are Fresnel coefficients that depend on the azimuthal angle of incidence and on the dielectric constants of the two phases that constitute the interface. The important quantities are the three coefficients a, b, and d. The first term describes the effect of currents that are driven in the direction perpendicular to the surface; the corresponding coefficient $a(\nu)$ is generally a complex quantity. The second term is caused by currents parallel to the surface; for a perfectly flat and structureless metal surface $b(\nu) = -1$. The third term is actually a bulk contribution: the incident light penetrates a short distance into the metal, and the magnetic dipole term, which is not symmetry forbidden, contributes to the signal with an amplitude $d(\nu) = 1$. To our present knowledge aqueous solutions make no direct contribution to the signal, unless adsorbates with a strong nonlinear polarizability are present. The presence of the solvent and of adsorbates can, however, modify the electronic properties of the metal surface, and thereby the SH response.

The coefficient $a(\nu)$, which characterizes the currents flowing perpendicular to the surface, is highly sensitive to the electronic structure of the interface. It is caused by the response of the surface electrons to an external field, an effect that we have already encountered when we discussed the contribution of the metal to the interfacial capacity. As was illustrated in Figure 7 an external field deforms the electronic density profile at the surface. This response has a strong nonlinear component, as is evident from the dependence of the effective image plane position on the surface charge density (see Figure 10). In effect, the surface electrons are being driven by the incident laser light, and the nonlinear part of their response gives rise to light at the second harmonic frequency. At low frequencies, in the *quasistatic limit*, the corresponding amplitude $a(\nu)$ is independent of the frequency and determined by the change of the effective image plane position with the external field or, equivalently, with the surface charge density σ:[21,39]

$$a = 2n_b\left[2\frac{dx_{im}}{d\sigma} + \sigma\frac{d^2x_{im}}{d\sigma^2}\right] \quad (12)$$

In essence, the effective position of the image plane governs the linear electronic response of the interface, and its rate of change with the field governs its nonlinear response.

At higher laser frequencies the electronic response is not in phase with the incident light and must be calculated by the time-dependent density functional formalism. This was achieved by Liebsch and others[39,40] in a series of papers using jellium as a model for the metal. While jellium does not account for band-structure effects or for surface states (see below), it represents the response of the surface electrons to an external field well, as long as there are no resonances.

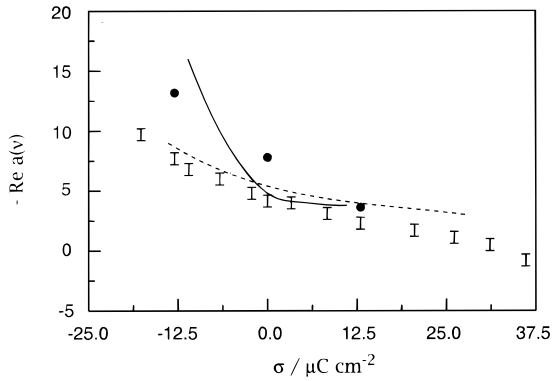

Figure 16. Real part of the coefficient $a(\nu)$ for a Ag(111) electrode as a function of the charge density. The error bars are the values from Guyot-Sionnest et al.;[41] the three points are the values recalculated by Furtak et al.;[44] the full line is the theoretical curve from ref 42; and the dashed line is the theoretical curve from ref 41 scaled by a factor of 0.3 as explained in the text.

The observed signal arises through the interference of three terms (see eq 11). This makes it difficult to extract the coefficients $a(\nu)$, $b(\nu)$, and $d(\nu)$, which are required for a detailed comparison between theory and experiment, from the experimental data. In a pioneering paper Guyot-Sionnest, Tadjeddine, and Liebsch[41] measured the SH response of a Ag(111) electrode in a 0.1 M solution of $KClO_4$ at various angles of incident over a range of potentials. Assuming the theoretical values of $b(\nu) = -1$ and $d(\nu) = 1$, they obtained quasiexperimental values for $a(\nu)$ by a fitting procedure. Figure 16 shows the resulting values as a function of the charge density on the electrode; the wavelength of the employed laser beam was 1064 nm, which is far from any interband transition. The real part of the coefficent a is negative over the range that is shown, and its absolute value decreases from negative toward positive charge densities. The data presented in the original paper were later examined by Furtak at al.;[44] they pointed out that the fomula employed by Guyot-Sionnnest et al. contains a small error; the correct values for $-\mathrm{Re}(a)$ are somewhat higher. Theoretical values, based on the jellium model and assuming one free electron per silver atom, result in a curve with the same overall trend, but the values for $-\mathrm{Re}(a)$ are substantially too high. A three-dimensional quantum-chemical calculation by Aers and Inglesfield[28] gives a value of $a = -8.83$ au for Ag(100) in the quasistatic limit. This is about 0.3 times the value obtained from the jellium model, which does not contain lattice structure, and hence does not distinguish between Ag(111) and Ag(100). If the theoretical curve is scaled by this factor of 0.3—thus accounting for structure in a phenomenological way—it passes closer to the theoretical points.

In a later investigation Leiva and Schmickler[42] used jellium with pseudopotentials to account for the

effect of the lattice structure. Their calculations, performed for the quasistaic limit, predict significant differences between the SH response of different single crystal surfaces. For silver in contact with an aqueous solution they employed the model of Russier and Badiali[24] and used the optical dielectric constant of water (see section 3.2). Their theoretical curve for Ag(111), which is free of any adjustable parameter, passes close to the experimental points, except for the region of highly negative charge densities, where it predicts too high values for $-\mathrm{Re}(a)$.

All variants of the jellium model that have been used so far predict a strong increase of $-\mathrm{Re}(a)$ at negative charge densities because the electrons spill out further and their nonlinear response becomes stronger. The experimental data do show an increase, but it is not as strong as predicted by the theory. The problem lies probably with the interaction of the jellium tail with water, which becomes stronger as the electrons penetrate further into the solution but is not well represented in these conceptually simple models. In addition, there is some indication that the coefficient $b(\nu)$ may differ from the theoretical value of -1.[43]

When SHG is performed at a fixed frequency of the incident light one can obtain interesting information about the electronic response at the surface, but not about energy levels. In order to use SHG as a spectroscopic probe one has to vary the wavelength of the incident light. A major feature is expected whenever the energy of an incident photon or of a SH photon is in resonance with an electronic transition at the surface that is not forbidden by symmetry. As an example we consider SHG from a Ag(111) surface immersed in an aqueous solution. When a p-polarized beam is incident on the surface, the p-polarized output signal, plotted as a function of the incident frequency, is rather featureless. In contrast, the s-polarized SH signal shows a marked maximum at a SH photon energy of about 3.82 eV. The height of this maximum depends on the electrode potential and is higher at negative charges; its position remains unchanged (see Figure 17).

The nature of the corresponding electronic transition is still a matter of debate. The initial state is probably a surface state that, in vacuum, is located 120 meV below the Fermi level at the $\bar{\Gamma}$ in the surface Brillouin zone. When the electrode potential is varied the energy of the surface state will change (see the discussion in section 4.1), and so will its occupancy. On the application of a negative potential the state is pushed further below the Fermi level, its occupation increases, and the resonance should be enhanced, which is in line with the experimental data. Since the resonance does not disappear over the investigated range of potentials, its shift in energy must be smaller than its width. Two different candidates have been proposed for the final state: Bradley et al.[43] argue that the the transition occurs to the unoccupied bulk band edge, while Furtak et al.[44] assume that the final state is an image potential state.

Performing electronic surface spectroscopy by SHG is difficult and costly; therefore, this technique has not been widely applied.

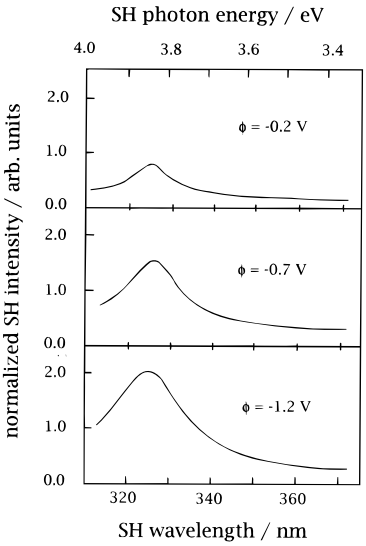

Figure 17. Wavelength dependence of the normalized SH intensity from Ag(111) in contact with a solution of 0.1 $NaClO_4$ for p-input and s-output polarization. The angle of incidence was 30°; the electrode potential is given with respect to Ag/AgCl; the pzc is near -0.7 V. Adapted from ref 43 with permission.

5. Surface Reconstruction

At the surface of a solid metal the three-dimensional translation symmetry of its lattice is abruptly broken, and the surface atoms have fewer neighbors than those in the bulk. Therefore, the surface atoms may rearrange to form a surface that is denser than that of the ideally terminated lattice; this process is called *reconstruction*. However, this tendency is opposed by the interaction of the surface atoms with the second and third lattice plane, which favors the ideal structure. In addition, the surface structure is affected by the tendency of the surface electrons to spread over a large volume in order to minimize their kinetic energy. Whether surface reconstruction takes place or not depends on the balance between these forces. A number of metal surfaces, for example, the (100) surfaces of Ir, Pt, and Au, are known to reconstruct in vacuo. However, the adsorption of atoms or molecules frequently lifts the reconstruction, particularly if they are electronegative (see, for example, refs 45, 46, and 51), because a strong metal−adsorbate interaction favors a more open surface. In other instances, the adsorption of electron donors may induce reconstruction.

Among the surfaces that reconstruct in vacuum are the three principle planes of single-crystal gold electrodes, and these have been the focus of several electrochemical studies (for recent reviews see refs 47 and 48). We consider the Au(110) and Au(100) surfaces in greater detail. A freshly prepared, flame-annealed Au(110) surface shows a so-called 1×2 or *missing row* reconstruction (see Figure 18) in vacuo, in which every other row is missing.[59,60] The adsorption of submonolayers of Cs and K, which donate electrons to the substrate, induces a 1×3 reconstruction on Au(110) surfaces,[57,58] in which the outer atoms are shifted inward, so that the surface becomes denser; this is indicated by the arrows in Figure 18. Conversely, the adsorption of electronegative atoms or molecules lifts the reconstruction, and the surface

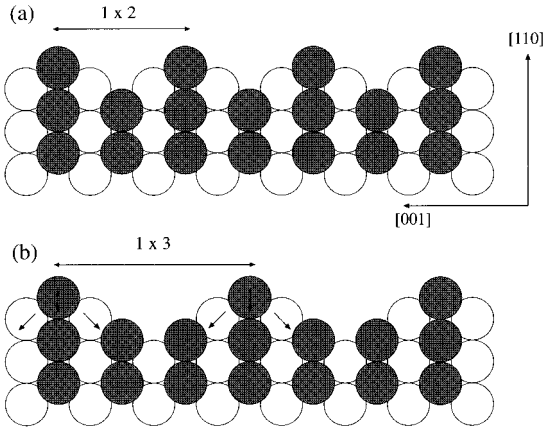

Figure 18. Surface structure of reconstructed Au(110) surfaces (schematic): (a) 1 × 2 structure, (b) 1 × 3 structure; the arrows denote a displacement of the surface atoms.

returns to the ideal 1 × 1 structure. Obviously, the donation of electrons to the surface favors a reconstruction, while a detraction of electrons lifts it.

In electrochemical systems the density of electrons at the surface can be controlled directly through the electrode potential without necessarily involving the adsorption of other species. By surface X-ray scattering, Ocko et al.[54] observed the Au(110) 1 × 3 reconstructed surface in salt solutions at potentials well below the potential of zero charge. A careful analysis of their data revealed the relaxation of the top surface layer discussed above. In acid solutions, where one cannot perform experiments at high negative charges because of hydrogen evolution, this group observed a poorly correlated structure intermediate between 1 × 3 and 1 × 2. An STM study of acid solutions by Magnussen et al.[55] revealed a 1 × 2 structure with a large density of defects at negative potentials, while at potentials above 0.2 V vs SCE, where the electrode is positively charged, the reconstruction is removed. An earlier study by Gao et al.[56] had shown both 1 × 2 and 1 × 3 structures at negative potentials. So the electrochemical investigations show a transition series, (1 × 3) → (1 × 2) → (1 × 1), as the surface charge increases from negative toward positive values, which is in line with the observations in the uhv.

These experimental findings can be explained in terms of model calculations for the Ag(110)[52] and Au(110)[53] surfaces. Figure 19 shows calculated values for the surface energies of the ideal (1 × 1) and the 1 × 2 and 1 × 3 surfaces as a function of the charge per surface atom. (Actually, the curves in this figure do not show the true surface energies, because contributions from the counter charge have been included; however, only the difference between the curves is relevant for our argument.) The differences between the three curves are quite small, so that a relatively minor change of the system parameters may induce or lift a reconstruction. For an uncharged surface the 1 × 3 reconstruction has the lowest energy. With increasing positive charge at first the 1 × 2 and then the ideal 1 × 1 surfaces become more favorable. These changes can be explained in terms of the tendency of the surface electrons to occupy a large volume, thus decreasing

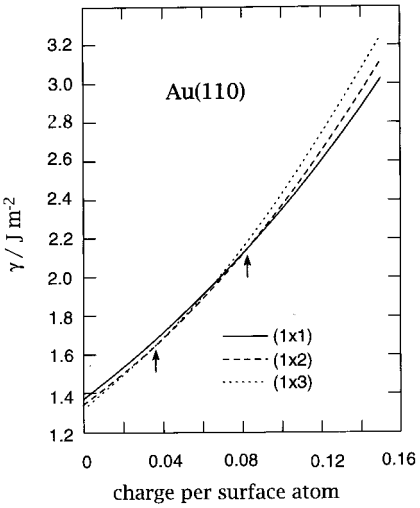

Figure 19. Surface energy γ of an ideal Au(110) surface (solid line) and a surface with a 1 × 2 reconstruction.[53] The arrows indicate the intersection points of the curves.

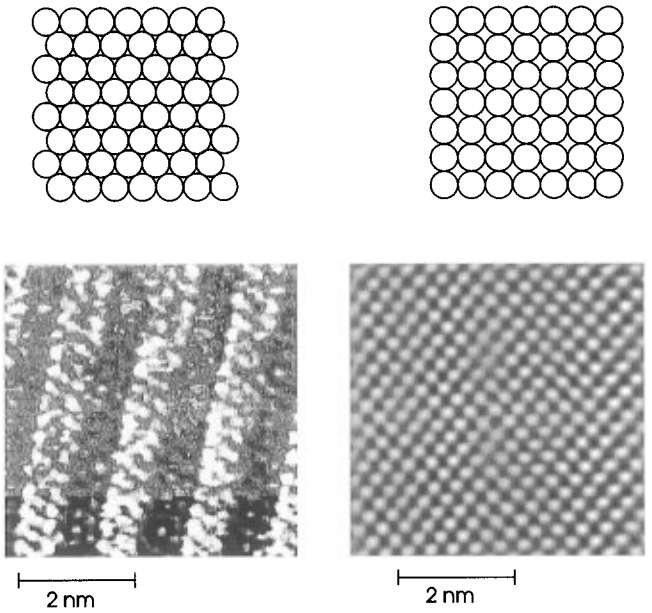

Figure 20. Surface structure of the reconstructed (left) and of the ideal (right) Au(100) surface. The upper drawings show the surface structures of the STM images below. On account of the misfit of the top layer with the bulk the reconstructed surface shows a surface corrugation. Courtesy of D. M. Kolb, Ulm.

their kinetic energy. The 1 × 3 surface is fairly open and allows the electrons to extend into the region between the top atom rows. To a lesser extent this is also true of the 1 × 2 reconstructed surface. Therefore, an increase of electronic density at the surface favors the missing row reconstructions.

A similar, but somewhat simpler, situation occurs at the Au(100) surface. A freshly prepared surface shows a hexagonal surface reconstruction in vacuo. When such a surface is immersed into an aqueous electrolyte solution at a potential well below the potential of zero charge, the reconstruction remains intact and can be observed with a scanning tunneling microscope (see Figure 20) and with X-ray scattering techniques.[49] When the potential is subsequently scanned in the positive direction the reconstruction

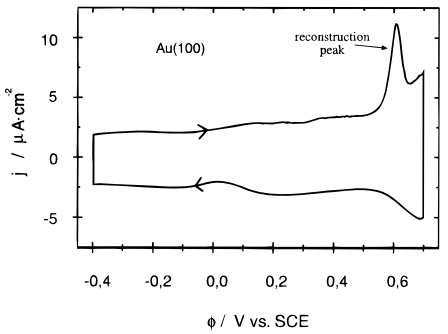

Figure 21. Current/potential curve (cyclic voltammogram) of a Au(100) surface in 10 mM $HClO_4$. The electrode has been prepared by flame annealing and was then immersed into the solution at a potantial of −0.4 V vs SCE. Subsequently, the potential was scanned with a rate of 50 mV s^{-1} in the positive direction. At a potential of 0.7 V the direction of the sweep was reversed until the initial potential was reached again. The direction of the scan is indicated by an arrow.

is lifted, and the ideal surface structure appears. In a current−potential scan this lifting is seen as a current peak (see Figure 21). Since the potential of zero charge of the reconstructed surface lies substantially above that of the ideal surface[50] the electrode is charged positive during the transition. The potential at which this phase transition occurs depends on the composition of the solution. For example, in a solution of 0.1 M H_2SO_4, where the anions are only weakly adsorbed, the reconstruction is lifted at a potential of about 0.6 V vs SCE (saturated calomel electrode); the addition of only 0.1 mM HCl shifts this potential to a value of 0.4 V. Since the chloride ion is strongly adsorbed, it seems that the specific adsorption of anions favors the more open ideal surface. This is in line with the observations in the uhv mentioned above.

When the potential is scanned back in the negative direction electronic charge is accumulated on the metal surface, and the electrode surface undergoes reconstruction at a potential well to the negative of the pzc, as is evident from the current peak. However, this return to the original reconstructed surface is slow because it is kinetically hindered; therefore, it does not show up as a narrow current peak.

So the electrochemical interface offers the unique capability to induce or lift surface reconstructions in a number of systems simply by changing the electrode potential. Though these surface phase transitions are often accompanied by the specific adsorption of ions, which may shift the transition potential to some extent, the driving mechanism seems to be the accumulation or depletion of electronic charge on the electrode surface.

6. Resistance of Thin Electrodes

When the working electrode consists of a thin film with a thickness in the micrometer range its resistance parallel to the surface is sensitive to the electronic structure of the surface. The essence of this effect can be understood within a free electron model, in which the bulk resistivity ρ_b of a metal with an electronic density n_b is given by the equation[61]

$$\rho_b = \frac{\hbar k_f}{e_0^2 n_b l} \tag{13}$$

where k_f is the Fermi wave vector and l is the mean free path of the electrons. When the thickness of the film is comparable to the mean free path, boundary effects become important. In a simple model the electrons impinge on the boundary where they are reflected. This reflection can either be specular or diffuse. If we denote by p_u and p_l the probability that the electron undergoes specular reflection at the upper or lower surface, respectively, the resistivity ρ of a thin film can be written in the form[62]

$$\rho = \rho_b\left[1 - \frac{3}{4\kappa}\int_0^1 \frac{(u - u^3)[1 - \exp(-\kappa/u)]}{1 - p_u p_l \exp(-2\kappa/u)}[2 - p_u - p_l + (p_u + p_l - 2p_u p_l)\exp(\kappa/u)]\,du\right]^{-1} \tag{14}$$

where κ is the ratio of the film thickness to the mean free path of the electrons; the integral is performed over all values of the cosine u of the angle of incidence of the electron on the surface. Strictly speaking, the specularity parameters of the surface depend on the angle of incidence. It is, however, instructive to take them as constant and plot the relative resistivity ρ/ρ_b against this parameter. As one expects, the resistance is the higher, the smaller the degree of specularity, and the thinner the film (see Figure 22). Conversely, if all electrons are specularly reflected ($p_b = p_l = 1$), the boundary does not affect the resistivity.

The presence of adsorbates alters the electronic properties of the electrode surface and hence affects the resistivity. The interpretation is simplest in the case of nonmetallic adsorbates such as the halide ions. Essentially, such adsorbates serve as scattering centers for the conduction electrons and decrease the degree of specularity of the electrode surface.[63,64] This entails an increase of the resistance, which, over a broad range of coverages, is proportional to the amount adsorbed.

As an example we consider the adsorption of chloride ions an a thin Au(111) electrode.[65] When the electrode potential is scanned from a negative value, at which there is no specific adsorption, in the positive direction, the adsorption of chloride ions shows up as a peak in the current flowing through the interface (see Figure 23a). Simultaneously, the resistance of the electrode parallel to the surface increases. When the potential is scanned back in the negative direction, the desorption is observed as a cathodic current peak and a simultaneous decrease of the resistance, both occurring with a small hysteresis. The rate of change of the resistance should be proportional to the change in the coverage and, hence, to that part of the current that is due to the adsorption. This is indeed the case (see Figure 23c). In contrast to the current, the change in the resistance is not affected by the charging of the double layer, or by hydrogen evolution; therefore, it gives precise information on the adsorption process.

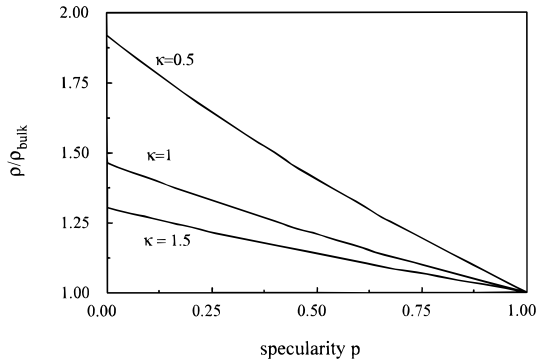

Figure 22. Relative resistivity of a thin film as a function of the specularity for $p_u = p_l = p$.

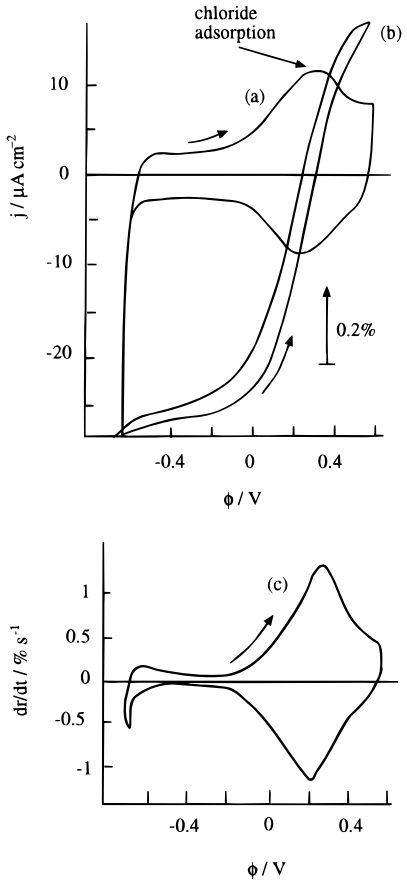

Figure 23. (a) Current and (b) resistance change during the adsorption of chloride ions; (c) rate of change of the resistance. The electrode was a Au(111) film with a thickness of 150 nm, the electrolyte was an aqueous solution of 50 μM NaCl and 10 mM $HClO_4$; for clarity the noise shown in the original data has been smoothed. The scale for part b is indicated by the adjacent arrow. Adapted from ref 65 by courtesy of Elsevier.

7. Tunneling of Electrons through the Electric Double Layer

The development of the scanning tunneling microscope (STM) for use in electrochemical cells was one of the significant advances in experimental techniques during the past decade. A fair number of electrode surfaces, both pure and adsorbate-covered, have been imaged with atomic resolution and provided a wealth of detailed microscopic information, which is rivaled only by in situ surface X-ray scattering techniques. However, here we are not concerned with the imaging of the electrode surface, but

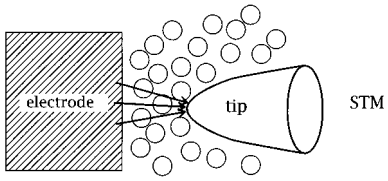

Figure 24. Electron tunneling through the double layer in the STM configuration.

with the physical process on which it is based: the tunneling of electrons through the double layer between the electrode surface and the STM tip (see Figure 24).

The presence of water has little effect on the STM images of clean metal surfaces, so electrons can tunnel through water and aqueous solutions. However, the variation of the STM current with the distance between the metal surface and the tip is markedly different. This dependence can be characterized by the *effective barrier height* for electron tunneling. Its definition is based on the simple Gamov formula, according to which the probability P_t that a particle of mass m tunnels through a potential energy barrier of a constant height V_b and thickness l is given by:

$$P_t = \exp\left(-\frac{2}{\hbar}\sqrt{2mV_b}\, l\right) \tag{15}$$

Of course, the barrier height for the tunneling of electrons through water is not constant; in addition, the absolute value of the separation l between the tip and the substrate cannot be measured with the required precision. However, the tunneling current can measured as a function of the change of the separation. This makes it convenient to define the effective barrier height through

$$V_b = -\frac{\hbar^2}{8m}\left(\frac{\mathrm{d}\ln i}{\mathrm{d}\, l}\right)^2 \tag{16}$$

where i is the tunneling current.

We will first consider the situation in vacuo, which is not complicated by the presence of water. At a small bias potential ΔV between the tip and the substrate the electrons will tunnel from the metal with the higher Fermi level to that with the lower one. At $T = 0$ the available energy range is $e_0\Delta V$; at room temperature there is some thermal smearing of the order kT, which is negligible for most purposes. Since the work function of a metal gives the energy required for an electron to leave the surface, we can expect the effective barrier height to be of the order of the average work function of the metal and, therefore, in the range of 4−5 eV. Typical experiments in vacuo show indeed an approximately exponential dependence of the tunneling current on the separation, which is in accord with eq 15, but due to electronic interactions between the two metals the effective barrier height is usually a little lower than the work function.

The corresponding experiments in solutions are difficult to perform. The high field between the tip and the substrate attracts impurities as the tip scans over the surface. So it is not surprising that experimental values for the effective barrier height for

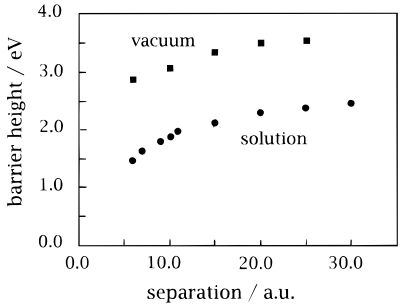

Figure 25. Effective barrier height as a function of the metal-tip separation in a simple one-dimensional model;[71] 1 au 0.529 Å.

electron tunneling through water show some scatter. They seem to fall into two classes: low values in the range of a few tenths of an electron volt (e.g., refs 66 and 67) and higher values of 1−2 eV.[68−70] In any case, the barrier height is substantially lower than in vacuum.

These experimental findings provoked some theoretical work to explain the enhanced tunneling rate in the presence of water. In an early paper Schmickler and Henderson[71] considered a model system consisting of a flat metal electrode modeled as jellium, a metal tip modeled as a jellium sphere, and an intervening dielectric representing the water. The tunneling electron interacts with the electronic polarizability of water, thereby reducing the barrier height by about 1 eV. This mechanism is similar to one observed in electron emission into water: the work function for this process also lies about 1 eV below the vacuum value.[72] The resulting barrier heights are of the order 2−3 eV and, thus, still somewhat higher than the experimental values (see Figure 25).

The same mechanism was further explored by Sebastian and Doyen[73] and by Rostkier-Edelstein et al.,[74] who in addition examined the effect of thermal fluctuations on the tunneling current. The former authors estimated that these fluctuations should have little influence on the barrier height, the latter concluded that they enhance the current.

Other groups have proposed that the electrons tunnels via one or several intermediate states; this mechanism would reduce the apparent barrier height even further. This can be seen from the following argument: The tunneling probability P_t^i for an exchange via an intermediate state is given by:

$$P_t^{\,i} = \frac{P_t(m-i)P_t(i-t)}{P_t(m-i)+P_t(i-t)} \qquad (17)$$

where $P_t(m-i)$ is the tunneling probability from the metal electrode to the intermediate state and $P_t(i-t)$ the tunneling probability from the latter to the tip. Both probabilites are given by a Gamov-type formula like eq 15. It is easy to see that P_t^i is governed by the smaller of the two tunneling probabilities $P_t(m-i)$ and $P_t(i-t)$; the most favorable case occurs if the two are equal. When the tunneling gap is changed by an amount Δl the position of the intermediate state will typically vary only by a fraction of Δl, or even not at all. Consequently, the apparent barrier height, as defined by eq 16, will seem much smaller than the actual height.

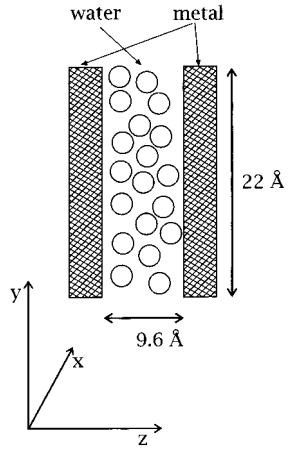

Figure 26. Model for calculating tunneling probabilities.[77]

The problem with this argument is that, under the usual operating conditions, there are no electronic states in water that lie anywhere near the Fermi level of the electrodes. Sass and Gimzewski[75] proposed hydrated electrons as intermediate states. However, the formation of hydrated electrons requires an energy of activation of about 0.5 eV, and they have a radius of about 10 Å, so that they would not even fit into the tunneling gap. This makes tunneling via these states rather unlikely.

Halbritter et al.[76] invoke dipole resonances as intermediate states. They are supposed to arise from the Coulomb interaction of the electron with the dipole moment of water; we will return to this point below. They explain their very low values for the barrier height by tunneling through multiple intermediate states. The basis of their argument is the following: If the electron tunnels through one intermediate state that always lies right at the center of the barrier, the apparent barrier height is half the real height; this can be seen from eq 17. Similarly, if there are n states that are always at equal distances through the barrier, the apparent barrier height is lowered by a factor of $(n+1)$. In this way they explain barrier heights of the order of a few tenths of an electron volt as being caused by tunneling via five to six such states. Again, such a mechanism seems highly unlikely. Whatever the nature of these dipole resonces may be, their energies must lie substantially above the Fermi level. With a tunnel gap of the order of a few angstroms, tunneling via a series of such states must have a much lower probability than direct tunneling.

The most elaborate models to date were devised by Schmickler[77] and by Mosyak, Nitzan, and Kosloff.[78] We describe our own work first. Both the electrode and the tip are modeled as semiinfinite jellium (see Figure 26). The gap between the two jellium edges is filled with water molecules; its thickness was adjusted to 9.6 Å so that it contains three layers of molecules. By use of the central force model for water,[79] molecular dynamics simulations were performed. When these had proceeded for some time the water configuration was recorded. The interaction potential between the tunneling electron and this water layer was calculated from the electron−

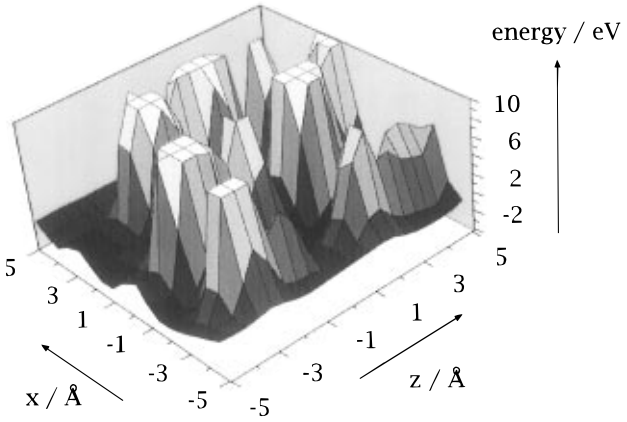

Figure 27. Cross-section ($y = 0$) through the three-dimensional potential energy surface generated by the water layer. The coordinate system is shown in Figure 26. For clarity the potential was cut off at 10 eV. The maxima correspond to the positions of oxygen atoms, the minima to hydrogen atoms.

water pseudopotential devised by Barnett et al.[80] The resulting three-dimensional potential energy surface has pronounced maxima at the positions of the oxygen atoms and shallow minima near the hydrogen atoms—a cross-section through such a surface is shown in Figure 27. To obtain the total interaction potential the contribution from the jellium is added.

In this model the tunneling electrons experience a strongly varying potential. The tunneling process itself can be visualized as the scattering of an incoming wavepacket by this potential. In order to calculate the tunneling probability a window of 6 Å × 6 Å perpendicular to the z direction (see Figure 26) was chosen at random, and cyclic boundary conditions were imposed in the x and y directions. A Fourier transformation in the x and y coordinates results in a coupled system of one-dimensional Schrödinger equations in the z coordinate, which was solved numerically with the boundary conditions appropriate for the scattering of a particle incident from the left:

$$\text{at } z = -\infty\text{: incoming wave } \exp ikz + \text{reflected wave}$$

$$\text{at } z = \infty\text{: outgoing wave}$$

These calculations were repeated for a large number of water configurations. A few typical results are shown in Figure 28. For the 6 Å × 6 Å window the tunneling probabilities are of the order of 10^{-7}—10^{-6} and fluctuate by about a factor of 10.

If the average tunneling probability it substituted into the Gamov formula one obtains an effective barrier height of about 2 eV. However, experimental barrier heights are not obtained from the absolute value of the tunneling probabilty but from a variation of the tunneling gap. So, this theoretical value for the barrier height does not quite correspond to the quantity that is measured experimentally.

The work by Mosyak et al. is similar in many respects. This group also calculates the tunneling probability trough three layes of water sandwiched between two electrodes. The water model, and the interaction of the water with the electrode, are

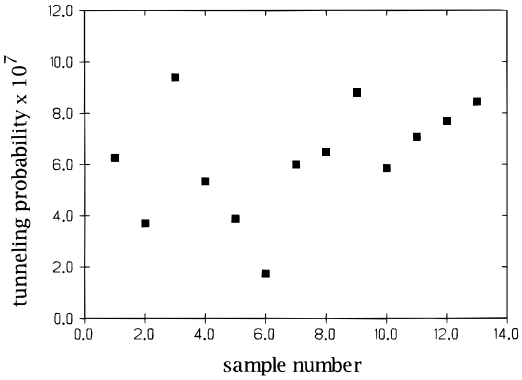

Figure 28. Tunneling probability for various configurations of the interveneing water layer.[77]

somewhat different, but the same electron—water pseudopotential is employed. The model for the electrode is simpler: The space between the two plates has an additional vacuum potential of 5 eV, which drops to zero at the two metal surfaces. The Fermi level of the electrode from which tunneling occurs is taken as 3.5 eV. Thus, the gradual increase of the jellium potential and its decrease due to the interaction with the electronic polarizability are absent in this model, but the average contribution of the metal to the tunneling barrier is very similar to that in our work, and the tunneling probabilities, which were calculated by three different methods, lie in the same range. The results are compared to one-dimensional models, which are found to be inadequate. Given the complicated shape of the full potential energy surface, with its maxima at the oxygen atoms and the minima at the hydrogen atoms, this is not surprising. The same group has recently investigated the effect of the polarizability of water on the tunneling probability.[81] The water pseudopotential by Barnett et al. contains a term for the interaction of the electron with the electronic polarizability of a single water molecule, but not the effect of that polarizability on the water—water interaction. If this effect is included in the model, the calculated tunneling rate is enhanced by about 2 orders of magnitude and gets closer to the experimental data.

In all of these works the electron is assumed to tunnel through a static barrier. This is justified by the different time scales for the tunneling of electrons, which for this type of barrier lies in the range of 10^{-16} s, and for the motion of water,[73] which is slower by at least 2 orders of magnitude.

While these three-dimensional models constitute a major advance over the continuum models, much work remains to be done. The dependence of the current on the width of the tunneling gap has still to be investigated. Also, the role of solvent fluctuations is not yet clear. In principle, it is possible that certain favorable solvent configurations exist that give rise to a very large tunneling probability. Though such fluctuations may be too rare to be observed by sampling the configurations produced by molecular dynamics, they could still make a large contribution to the total current.

The potential energy surfaces constructed through this approach also shed some light on the question of intermediate states. Neither we nor Mosyak et al.

observed any resonances that are close to the Fermi level. However, the potential energy surface has minima at the positions of the hydrogen atoms, which increase the tunneling probability. Lindsey et al.[82] have proposed a model in which the electron tunnels via a series of virtual intermediate states localized on the oxygen atoms. In view of the shape of the potential energy surfaces these states should rather be localized on the hydrogen atoms.

8. Electronic Effects on Electron Transfer Reactions

8.1. Outer-Sphere Electron Transfer Reactions

Electron transfer reactions are the simplest type of electrochemical reactions and have been the subject of intensive investigations. The theory is well developed for so-called *outer-sphere* electron transfer reactions, in which bonds are neither formed nor broken. In general, the rate constant for such a reaction can be written in the form

$$k = A \exp\frac{-G^{\ddagger}(\phi)}{kT} \qquad (18)$$

where $G^{\ddagger}$ is the Gibbs free energy of activation, and A a preexponential factor. According to the theory of Marcus[83] the Gibbs energy of activation $G^{\ddagger}$ depends on the energy required to reorganize the reacting complex and the surrounding solvation sphere and on the Gibbs energy of the reaction, which in turn depends on the electrode potential ϕ. In contrast, the preexponential factor A is assumed to be independent of the electrode potential. More recent theories for electrochemical electron transfer reactions predict a relation of the same form (see, e.g., refs 84 and 85).

The strength of the electronic interaction between the reactant and the metal must obviously affect the reaction rate. If the interaction is strong, the reaction is *adiabatic*, and the reaction rate is independent of the electronic interaction (for an experimental verification, see ref 86). At a first glance this may seem surprising, but it can be readily explained by the following consideration: The free energy surface for the reaction is determined by the reorganization of the reactants and of the solvation sphere and by the reaction free energy, none of which depend on the electronic overlap. If the electronic interaction is strong, an electron transfer takes place every time the system crosses the saddle point that separates the reactant and the product region, and the rate is independent of the electronic overlap. However, if the electronic interaction is weak, there is only a small probability that the electron will be exchanged when the system is on the saddle point and that probability depends on the electronic overlap. In the latter case the reaction is *nonadiabatic*.

In the nonadiabatic case the preexponential factor contains the electronic interaction between the reactant and the electrode[87] and may be taken as proportional to the electronic overlap S between the two reactants. Usually, S is assumed to be independent of the electrode potential. However, Kornyshev et al.[88] realized that on simple metals, for which jellium is a good model, the metal wave functions

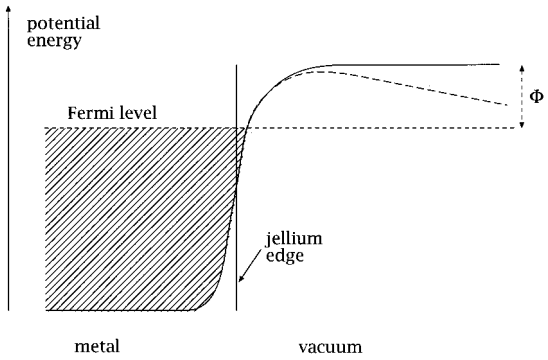

Figure 29. Potential energy experienced by an electron near the jellium edge (schematic). Full line: for an uncharged surface. Dashed line: for a negatively charged surface.

may vary considerably with the charge density on the metal and, hence, with the electrode potential.

The effect is estimated to be greater for negatively charged electrodes, so we consider this case in greater detail. We have observed in section 3 that the electronic density profile on a metal surface varies with its charge density. For the electronic overlap with a reactant the relevant quantity is not the total electronic density but the decay of the wavefunction of electrons with energies near the Fermi level. This is determined by the one-electron potential, which, within the jellium model, contains contributions from the interaction with the positive background representing the ions cores, with the other electrons, and with the external charge. Figure 29 shows this potential for an uncharged and for a negatively charged surface in vacuum. At the uncharged surface the potential becomes constant at distances larger than a few angstroms from the metal surface. The difference in energy between the Fermi level and the horizontal top of the barrier is the work function of the metal. If the surface carries a negative charge the potential decreases linearly at larger distance, because the electrons are attracted by the positive countercharge. At sufficiently high charges the barrier becomes so thin that the electrons tunnel into vacuum; this is the familiar phenomenon of *field emission*. In the presence of an aqueous solution the situation will be similar. However, the field at the surface of a charged electrode will be screened by the ions, and the potential will be constant at larger distances. Nevertheless, the potential barrier is much lower at negative charges, so that the decay of the electronic wavefunction in the solution is significantly reduced. Therefore, for nonadiabatic reactions, the preexponential factor is expected to become larger if the surface is charged negatively.

This scenario is supported by recent experimental results for the reduction of Zn^{2+} ions on a series of indium and thallium amalgams.[11,89] The composition of these amalgams, and hence their electronic properties, can be varied over a large range. The potential of zero charge varies continuously with the composition, so that a given reaction can be investigated for different charge densities at the same electrode potential. The reduction of Zn^{2+} occurs in two steps:

$$Zn^{2+} + e^{-} \rightarrow Zn^{+}$$

$$Zn^+ + e^- \rightarrow Zn(Hg)$$

The first step is a simple electron transfer reaction; its rate constant is small, so it should be nonadiabatic. The second step is the formation of the amalgam, and need not concern us here. Figure 30 shows the rate constant of the first step as a function of the charge density for three different potentials. In each case the rate constant follows the same pattern: at first the rate increases a little as the negative excess charge decreases, and then it drops off continuously. The sharp rise at the beginning of these curves is attributed to a change in the density of states at the Fermi level of these amalgams, while the decaying part is readily explained by the mechanism outlined above.

Whether this type of correlation holds for other systems as well remains to be seen. The overall effect is not large—a factor of 3−4 is not much in kinetics—and there are very few systems where the electronic properties can be varied so systematically. Nevertheless, a verification of this effect would be important, since it would shed light on the principles of electron transfer theories.

8.2. Reaction of Hot Electrons

When a metal electrode donates an electron to a reactant in the double layer, the energy of the transferring electron is usually close to the Fermi level. Thermal excitations are of the order of kT, so the density of electrons with energies of 0.1 eV or more above the Fermi level electrons is almost negligible at ambient temperatures. On the other hand, the transfer of electrons with energies below the Fermi level generally requires a higher energy of activation and, therefore, happens only rarely. However, when the electrode is part of a tunnel junction hot electrons can be produced, with energies substantially above the Fermi level. When they reach the surface they can react with suitable acceptors at potentials at which the exchange of thermal electrons is negligible.

The principle of the method, which was developed by Diesing et al.,[90] is shown in Figure 31. The tunnel junction consists of a metal film (Ag or Mg) covered with an oxide layer about 3 nm thick, on which a thin silver film (thickness about 15 nm) has been deposited. The latter is in contact with an electrolyte solution and serves as the working electrode. When a suitable bias is applied between the metal and the silver film electrons can tunnel through the thin oxide film. The majority of the tunneling electrons will have energies close to the Fermi level of the metal source, since electrons with lower energies experience a higher tunneling barrier. Most electrons tunnel through without loss of energy and, therefore, arrive in the silver film with a substantial excess of energy above the Fermi level of the electrode. Most of these hot electrons will lose energy by electron−electron scattering and excite secondary hot electrons in this process. A small fraction will reach the electrode surface without loss of energy, and others will relax down to the Fermi level. So, there is a current of hot electrons impinging on the electrode surface from the inside. They can be

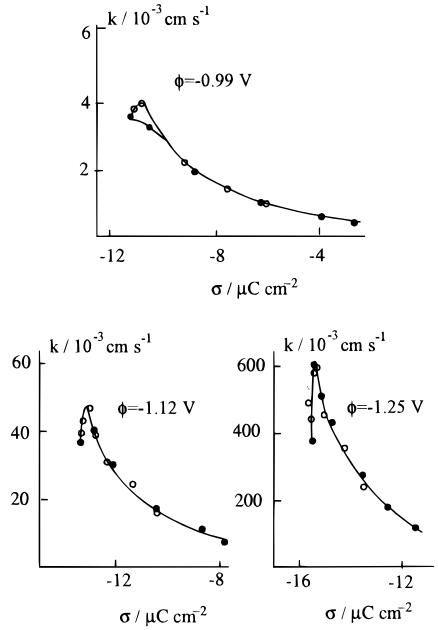

Figure 30. Rate constants for the reduction of Zn^2 on a series of amalgams as a function of the electrode charge density for three different electrode potentials.

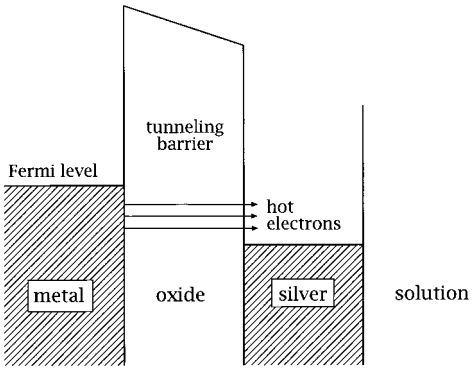

Figure 31. Generation of hot electrons by tunneling through an oxide film.

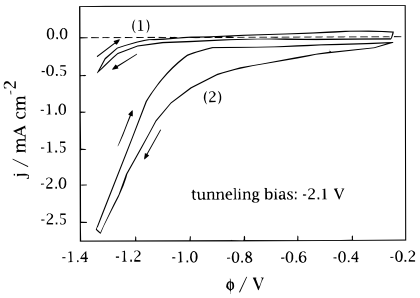

Figure 32. Cyclic voltammogram of a silver electrode without (1) and with (2) hot electrons.[90]

reflected back into the bulk, excite surface polaritons, and emit photons or react with suitable acceptors in the solution. The latter case is of interest here.

Curve 1 in Figure 32 shows a cyclic voltammogram of a polycrystalline silver electrode in an acetate buffer solution in the absence of hot electrons. The curve is flat and featureless over a wide range; at potentials below about −1.1 V vs SCE hydrogen evolution sets in. If a bias of −2.1 V is applied to the tunnel junction a tunneling current density of j_t = 14 mA cm^{-2} flows from the silver to the aluminum—the electrons, of course, flow in the op-

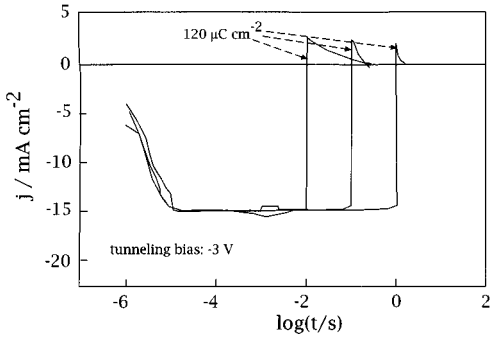

Figure 33. Current transients for the investigation of the reaction of hot electrons. The generation of hot electrons has been switched on at $t = 0$; the three curves correspond to different times of switching off the tunneling current.

posite direction. A sizable fraction of the induced hot electrons reaches the surface of the silver electrode where it can react with protons to form hydrogen. This is evident from curve 2 in Figure 32, where hydrogen evolution sets in at higher potentials than in the absence of hot electrons and is much enhanced. However, this effect is only observed if the electrodes are activated before the experiments by an oxidation−reduction cycle in a chloride-containing solution or by a similar procedure. The nature of this activation process, which is reminiscent of the activation required for the surface enhanced Raman effect, is not understood.

Further details about the hydrogen evolution reaction with hot electrons can be observed by pulse techniques. Figure 33 shows current transients for an electrode potential of −0.8 V vs SCE, at which under normal conditions no hydrogen evolution occurs. When the tunneling voltage is switched on at a time $t = 0$ the current rises quickly and reaches a steady state value after about 10^{-5} s. When the tunneling voltage is switched off the current drops abruptly, and a positive current transient is observed. For the three cases shown in Figure 33 the shape of this transient is independent of the duration of the tunneling current pulse (note that the time axis in Figure 33 is logarithmic). The total charge under these transients is about 120 μC cm^{-2}, which corresponds to roughly half a monolayer of silver atoms on a Ag(111) surface. A possible interpretation is the following: during the hydrogen evolution reaction adsorbed hydrogen occurs as an intermediate with a steady state coverage corresponding to 120 μC cm^{-2}. When the tunneling current is switched off these hydrogen atoms are reduced and give rise to the observed transient. These findings are surprising, because conventional wisdom holds—without much evidence—that the interaction of hydrogen with silver is too weak to form an adsorbed intermediate.

In any case, hot electrons offer a novel technique to investigate electrochemical reactions and promise to become an interesting field of study.

9. Models for the Electric Double Layer

So far we have focused our attention on those double layer properties that are governed by the metal electrons. A complete model of the interface must describe the electrons, the solvent, the ions, and the interactions of these constituents. This is a formidable task, and it is not surprising that is has not been solved yet. However, a few attempts at such complete models have been made. All of them stress the important role played by the metal electrons, but differ considerably in their treatment of the metal−solvent interaction. We will consider a few of these models in detail, discuss their differences, and point out the problems at which, in our view, future research should be directed.

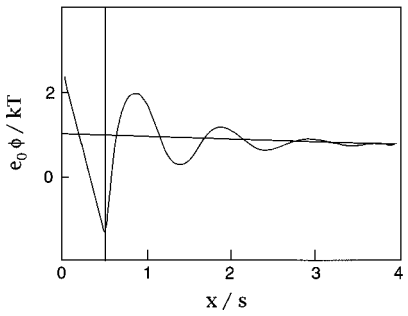

Figure 34. Distribution of the electrostatic potential for an ensemble of hard sphere ions and dipoles in contact with a hard wall situated at $x = 0$. The straight line is the prediction of the Gouy−Chapman theory. Adapted from ref 91 with permission.

9.1. The Jellium–Hard Sphere Electrolyte Model

Almost all the contemporary models use jellium, with or without pseudopotentials, as the model for the metal. The simplest molecular model for the solution is that of a *hard sphere electrolyte*, in which the solvent molecules are represented as hard spheres with a permanent dipole moment at their center, and the ions as charged hard spheres. The statistical mechanics even of this simple model are quite complicated. An approximate analytical solution has been obtained for the case where such an ensemble is in contact with a hard wall carrying a *small* excess charged density; i.e., the charge must be so small that linear response theory is applicable. It is based on the *mean spherical approximation*, which itself is a linearized theory. The mathematical details are given in the original papers by Carnie and Chan[91] and Blum and Henderson.[92] We briefly review the pertinent results.

Near the hard wall the density profile of the solvent molecules exhibits oscillations, whose amplitude decreases with the distance. They are caused by the finite size of the hard spheres—the same effect can be seen in any loose packing of spheres against a hard wall. Since the solvent molecules carry a dipole moment, these density oscillations give rise to concomitant oscillations in the electrostatic potential; they are shown in Figure 34 for the case where the solvent molecules and the ions have the same diameter. These oscillations do not occur in the Gouy−Chapman theory, which treats the ions as point particles and the solvent as a dielectric continuum. Therefore, an ensemble of hard sphere ions and dipoles in contact with a charged hard wall has a capacity which differs from the predictions of the Gouy−Chapman theory. However, the Gouy−Chapman theory, just like the Debye-Hückel theory, is exact in the limit of low ionic concentrations. Therefore, these deviations become noticeable only at higher concentrations.

Within the mean spherical approximation the inverse $1/C$ of the interfacial capacity can be expanded in powers of the Debye inverse length $\kappa = 1/L_D$. For the case where the anions and cations both carry unit charge and have the same diameter s as the solvent molecules, the first two terms are

$$C^{-1} = \frac{4\pi}{\epsilon\kappa} + \frac{2\pi s}{\epsilon}\left(1 + \frac{\epsilon - 1}{\lambda}\right) + ... \qquad (19)$$

where ϵ is the bulk dielectric constant of the solvent and λ is given by the equation

$$\lambda^2(1 + \lambda)^4 = 16\epsilon \qquad (20)$$

Since the calculations were performed for a small excess charge density, eq 19 gives the capacity at the pzc. As expected, the first term is the Gouy−Chapman capacity. The second term is independent of κ and hence of the electrolyte concentration; thus, it contributes to the Helmholtz capacity as defined in section 2.2. Higher order terms, which are not shown in eq 19, contain powers of κ and become important at high electrolyte concentrations; their effect seems to have been observed on mercury.[93]

It is the second term that is of interest to us here. The parameter λ characterizes the dielectric properties of the solvent near interfaces. For water, with $\epsilon = 78$, $\lambda \approx 2.65$. Therefore, in this model, the diameter of the ions has little effect on the Helmholtz capacity; it is dominated by the properties of the solvent. This is in line with experimental observations, which indicate that the Helmholtz capacity is independent of the nature of the ions, as long as they are not specifically adsorbed.

The simplest way to combine the hard sphere electrolyte with the jellium model is to identify the jellium edge with the hard wall in the calculation above.[94−97] If the only interaction of the jellium with the solution is the electrostatic interaction between the excess charges on the two sides on the interface, then the inverse Helmholtz capacity is simply the sum of two terms, the contributions of the metal and of the solution:

$$\frac{1}{C_H} = -\frac{x_{im}}{\epsilon_0} + \frac{2\pi s}{\epsilon}\left(1 + \frac{\epsilon - 1}{\lambda}\right) \qquad (21)$$

Again, this equation is only valid near the pzc. There is a numerical problem with this and with similar approaches: the inverse capacity appears as the difference between two terms of a similar order of magnitude. Nevertheless, if one takes the value for the image plane position for jellium in contact with a dielectric continuum with $\epsilon = 1.88$ as discussed in section 3.1, on obtains the dashed line in Figure 4a, which passes not far from the experimental points. Considering the fact that this is based on a model without any adjustable parameters the agreement is satisfactory.

A somewhat different approach was taken by Schmickler and Henderson.[96,97] They did not include the optical dielectric constant of water into their calculations, but assumed that the metal electrons are repelled by the water molecules. They took a simple repulsive potential of the form $V(z) = V_b z$ for $z > 0$ and fixed the value of the constant V_b such that the theoretical plot of $1/C_H$ vs n passes near the experimental points (see Figure 4a). The same procedure, but with different values for the repulsive constant V_b, can be applied to other solvents (see Figure 4b). Thus, this model has one free parameter, which must be adjusted for each solvent, and describes the dependence of the Helmholtz capacity at the pzc on the electronic density quantitatively. It should be noted that these calculations are based on an approximate variational solution for the electronic density profile and not on an exact solution; however, the approximation employed gives practically the same values for the position of the image plane as the exact procedure.[98]

The simple jellium model does not work for metals of the fourth and fifth column of the periodic table; for these elements the inclusion of pseudopotentials is essential. Using a simple variational solution for the electronic density profile, Leiva and Schmickler[99] obtained reasonable results for the capacity of polycrystalline Pb, Sn, Bi, and Sb electrodes.

In any case, it seems clear that this kind of model, without or with one adjustable parameter, correctly predicts both the order of magnitude of the Helmholtz capacity of simple metals and its dependence on the electronic density.

Since this simple approach works quite well for polycrystalline metals, it is natural to extend it to single crystal surfaces. However, the effective position of the image plane depends quite strongly on the crystal face (see Table 1). So, if one simply follows the method described above and identifies the jellium edge with the hard wall in the hard sphere electrolyte model, one obtains unreasonably large variations of the Helmholtz capacity at different surfaces. The best that can be said for this approach is that it gives the correct ordering of the Helmholtz capacity for the three principle crystal planes of silver.[100] There may be better choices for the position of the hard wall, but so far this question is unresolved. We will return to the problem of the separation between the metal and the solvent when we consider different approaches below.

As noted above, the properties of the hard sphere electrolyte could be calculated only for small excess charges, so that the results for the interfacial capacity are limited to the pzc. An extension of these results to higher charge densities has not been achieved. In order to explain the observed dependence of the Helmholtz capacity on the charge density Schmickler and Henderson have proposed a heuristic formula based on the following premises:

(1) At the pzc this formula should reduce to the known results.

(2) For very high fields the solvent dipoles should exhibit complete dielectric saturation.

(3) The interpolation between the cases of low and high fields should be effected by the Langevin function $L(x) = \coth x - 1/x$, which gives the thermally averaged orientation of a single free dipole in an external field.

These requirements define a unique interpolating formula for the contribution of the solvent to the interfacial capacity. The explicit formula is a little

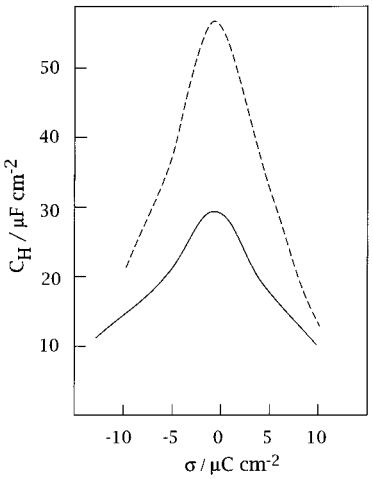

Figure 35. The Helmholtz capacity as function of the charge density. The dashed curve is for a bulk electronic density of $n_b = 0.02$ au, the full curve for $n_b = 0.01$ au; based on the work Schmickler and Henderson.[97]

bit cumbersome,[97] so we do not reproduce it here. A combination of this heuristic formula with the jellium model gives the type of capacity-charge characteristics that is shown in Figure 35. It shows a pronounced peak near the pzc; the decrease on both sides is caused by the dielectric saturation of the solvent. The overall shape of these theoretical curves is similar to that observed on silver and similar metals. This is pleasing, though such a heuristic approach cannot provide more than a qualitative explanation.

9.2. Models with a Variable Distance between the Metal and the Solution

As discussed above, the simple and natural assumption that the jellium edge provides a hard wall for the solution, seems to work well for polycrystalline metals but runs into problems with single crystal surfaces. Several groups have proposed that the distance between the metal surface and the first layer of solvent molecules should be calculated from the molecular interactions and that it varies with the surface charge density on the metal.[101−103]

Extensive model calculations based on this idea have been performed by the groups of Halley[104] and of Badiali.[105] Both groups try to calculate the equilibrium distance between jellium and a layer of solvent molecules from interaction potentials and obtain qualitatively similar results. We report on the work of Badiali et al. in greater detail.

This group considers two interactions between jellium and the solvent: an attractive van der Waals potential, which is calculated as the dispersion force, and a short-range repulsive interaction caused by the electronic overlap between jellium and the water molecules; the latter is calculated using a pseudopotential approach. We will not go into the details of these calculations—considering the complexity of the problem it is obvious that they must involve rather crude approximations, whose consequences are difficult to judge. Therefore, such calculations should not be considered as quantitative. Still, they are quite valuable since they point out where the difficulties lie and may serve as a basis for further improvements.

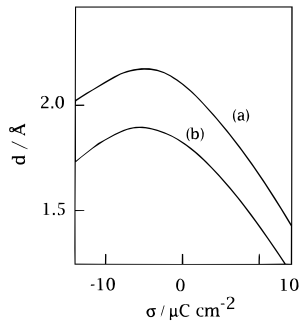

Figure 36. Variation of the distance of closest approach with the charge density; based on ref 105.

Once the interaction potentials have been estimated the equilibrium distance between the jellium edge and the water molecules can be obtained either by minimizing the free energy of the system or from pressure balance. In an exact calculation, both methods would give the same result, but this is not necessarily so in approximate calculations.

Amokrane and Badiali have performed model calculations for silver in contact with water using the pressure balance method. Interestingly, the distance d between the jellium edge and the center of the first layer of water molecules varies quite strongly in their model; this is in accord with the findings of Halley et al.[104] Figure 36 shows their results for an Ag(111) surface using two different assumed values of the water−jellium pseudopotential. Both curves have a similar shape: a maximum at slightly negative charge densities and a decrease at high positive or negative charges. This decrease is caused by the electrostatic pressure, which increases with the absolute value of the electric field. That the maximum is not at the pzc, but shifted toward negative charges, is due to the increased electronic spillover in this region. The shift of the metal−solvent distance with the charge density is surprisingly large, much larger than the change in the effective image plane position (cf. Figure 10).

Since in this model the distance between the jellium edge and the center of the solvent molecules is not equal to the radius s of the solvent molecules, and, in addition, changes with the charge density σ, the metal capacity must be defined differently. Amokrane and Badiali define it as

$$\frac{1}{C_m} = \frac{1}{\epsilon_0}\left[d - s + \sigma\frac{\partial d}{\partial \sigma} - x_{im}\right] \qquad (22)$$

The first two terms cancel if the jellium edge serves as a hard wall; since they relate both to the metal and the solvent, they might just as well have been incorporated into the solvent capacity. The third term vanishes if the distance d does not change, but in this model it makes a major contribution to the capacity.

To arrive at a complete double layer model, Amokrane and Badiali proceed in a semiempirical manner. Assuming that the contributions of the metal and the solvent to the inverse capacity are additive, they obtain the solvent capacity from experimental data for the Helmholtz capacity:

$$\frac{1}{C_s} = \frac{1}{C_H} - \frac{1}{C_m} \tag{23}$$

As experimental data they take the Helmholtz capacities for Ag(111) in contact with an aqueous solution of KF and for Ag(110) with a KPF_6 solution. Using the calculated values for the metal capacity—since these are based on the simple jellium model, they do not distinguish between different crystal planes—they then obtain the solvent capacity. Even though the experimental data for the two systems differ considerably at positive charges, the resulting semiempirical solvent capacity is almost the same (see Figure 37). This is due to the fact that the variation in the calculated metal capacity is much larger than the variation in any experimental data for the Helmholtz capacity. In fact, if the Helmholtz capacity had a constant value anywhere in the range of 20−100 μC cm^{-2}, or oscillated within this range, this procedure would still give essentially the same solvent capacity.

Still, the resulting solvent capacities have a reasonable shape: a maximum near the pzc, and a rapid, almost symmetric decrease at high field strengths, which is expected as a result of dielectric saturation. By adjusting a few parameters, the whole curve can be fitted to a model in which the solvent is represented by a monolayer of dipoles.

This kind of argument can be carried further: assuming that the solvent capacity is the same on all metal electrodes, one can obtain the capacities of metals other than silver from the experimental Helmholtz capacities by solving eq 23 for C_m. The resulting metal capacities show similar dependences on the electrode charge density (see Figure 38). Once these metal capacities have been calculated one can turn to other solvents and calculate their capacities using experimental data for the Helmholtz capacity. In this way one obtains the capacities of all metals and solvents for which the Helmholtz capacity is known. Again, all solvents show essentially the same behavior.

9.3. Discussion

The main breakthrough in our understanding of the electric double layer came in the early 1980s, when it transpired that the properties of this interface are governed by the response of both the metal electrons and the solution. The jellium model and its extensions provide a convenient framework for estimating the effect of external fields on the electronic distribution and the dipole potential of the interface. Comparison with experimental data shows that it gives both the correct order of magnitude for this effect and also the correct trends, in particular for the dependence on the bulk electron density and on the electrode charge. Much work has also been done on the structure of the solution at the interface. This falls beyond the scope of this paper; therefore, we have mentioned only the hard sphere electrolyte model. Here, the main point is the existence of an extended boundary layer, about 10−12 Å thick, in which the structure of the solvent differs from its bulk structure. The progress beyond the mean spherical approximation for the hard sphere electrolyte has been slow. There is still not even an approximate solution beyond the linear response to a surface charge. There has, however, been some progress in treating a model solvent and a single ion[106,107] by semianalytical techniques, and even more work in this direction has been performed by computer simulations (see, e.g., refs 108 and 109), but only very recently have attempts been made to combine such work with the jellium model in a consistent manner.[110]

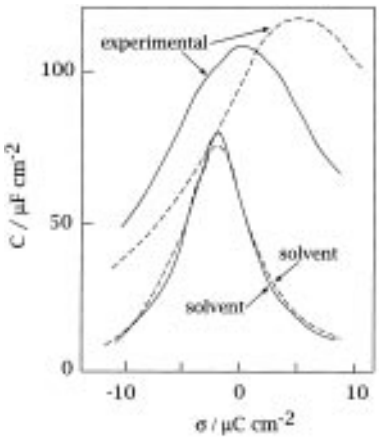

Figure 37. Solvent capacity for aqueous solutions according to the phenomenological theory of Amokrane and Badiali.[105] The full lines are from experimental data for a solution of KPF_6, the dashed curves for NaF.

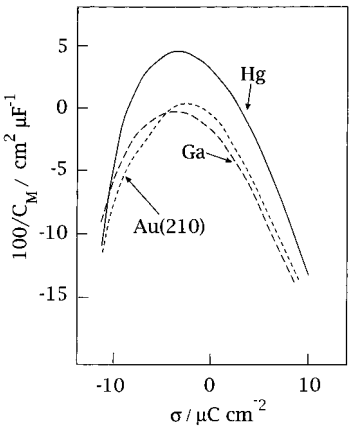

Figure 38. Inverse of the metal capacity according to ref 105.

The position of the first layer of water molecules with respect to the metal surface is still an open question. To choose the jellium edge as the dividing line, as was done by Schmickler and Henderson, is simple and gives good results for polycrystalline and liquid sp metal; it fails, however, for single crystals. The approach by Amokrane and Badiali is, in principle, preferable; but in our view is involves too many uncertainties in the interaction potentials and the approximations that have to be made, so that the results are not reliable. The large change in the metal−solvent distance that they and others obtain is surprising, and does not seem to be supported by experimental data.[111]

The field of double layer modeling is very active, and much that is written here may before long be overcome by new developments. The most ambitious work to date is that of Price and Halley,[112] who

develop a variant of the Car−Parinello method to calculate the structure of the metal−solution interface. However, this work is still in its infancy, and it is too early to decide whether it is even feasible.

10. Conclusion

It has been almost 50 years since Grahame published his famous article on *the electrochemical double layer and the theory of electrocapillarity* in *Chemical Reviews*.[113] At that time, double layer studies were rectricted to—highly precise—measurements of the interfacial tension of mercury electrodes, and the analysis was based on thermodynamics and some electrostatics. Despite, or because of, these limitations, Grahame's article is still fascinating to read; it possesses a coherence, an attention to detail, and a unifying view that is rare in modern scientific literature. With the exception of a few passages on the potential profile in the compact layer, his work has withstood the test of time, and nowadays it is being applied to solid single-crystal electrodes with great success.[114] In contrast, any modern review on the double layer necessarily presents a patchwork. We have a number of techniques that probe different aspects of the interface. Theory can explain certain effects and trends, in particular for sp and sd metals, but a unifying model of the double layer, which would encompass the electronic effects of the electrode, the structure of the solution at the interface, and their interactions, is still lacking. This makes the reading—and, indeed, the writing—of a review like this one less satisfactory. On the other hand, a subject that is well desribed by a unifying theory leaves little room for further research, so the present state of affairs should be taken as a sign that double layer studies are undergoing a rapid and healthy development.

11. References

(1) Lippmann, G. *Ann. Chim. Phys. (Paris)* **1975**, *5*, 494.
(2) von Helmholtz, H. L. *Wied. Ann.* **1879**, *7*, 337.
(3) Gouy, G. *J. Phys.* **1910**, *9*, 457
(4) Chapman, D. L. *Phil. Mag.* **1913**, *25*, 475.
(5) This kind of model is reviewed in: Reeves, R. In *Comprehensive Treatise of Electrochemistry, Vol. 1: The Electric Double Layer*; Bockris, J. O'M., Conway, B. E., Yeager, E., Eds.; Plenum Press: New York, 1980.
(6) Rice, O. K. *Phys. Rev.* **1928**, *31*, 105.
(7) Trasatti, S. In *Advances in Electrochemistry and Electrochemical Engineering*; Gerischer, H., Tobias, C. W., Eds.; Wiley Interscience: New York, 1977; Vol. 10, pp 213−321.
(8) Schmickler, W. *Interfacial Electrochemistry*; Oxford University Press: New York, 1996.
(9) Trasatti, S. In *Electrified Interfaces in Physics, Chemistry and Biology*; Guidelli, R., Ed.; NATO ASI Series; Kluwer Academic Publishers: Dordrecht, 1992.
(10) de Levie, R. *J. Electroanal. Chem.* **1990**, *280*, 179.
(11) Koene, L. Ph.D. thesis, University of Utrecht, 1995.
(12) Parsons, R.; Zobel, F. G. R. *J. Electroanal. Chem.* **1965**, *9*, 333.
(13) Badiali, J. P.; Rosinberg, M. L.; Goodisman, J. *J. Electroanal. Chem.* **1983**, *143*, 73; **1983**, *150*, 25.
(14) Schmickler, W. *J. Electroanal. Chem.* 1983, 150, 19.
(15) Smith, J. R. *Phys. Rev.* **1969**, *181*, 522.
(16) Lang, N. D.; Kohn, W. *Phys. Rev. B* **1970**, *1*, 4555; **1971**, *3*, 1215.
(17) Hohenberg, P.; Kohn, W. *Phys. Rev.* **1964**, *136*, B864; Kohn, W.; Sham, L. J. *Phys. Rev.* **1965**, *140*, A1133.
(18) Schmickler, W.; Henderson, D. J. *Phys. Rev. B* **1984**, *30*, 3081.
(19) Friedel, J. *Adv. Phys.* **1954**, *3*, 346.
(20) Lang, N. D.; Kohn, W. *Phys. Rev. B* **1973**, *7*, 2541.
(21) Schmickler, W.; Urbach, M. *Phys. Rev. B* **1993**, *47*, 6644.
(22) Ashcroft, N. E. *Phys. Rev. Lett.* **1966**, *23*, 48.
(23) Monnier, R.; Perdew, J. P. *Phys. Rev. B* **1978**, *17*, 2595.
(24) Russier, V.; Badiali, J. P. *Phys. Rev. B* **1989**, *39*, 13193.
(25) Leiva, E. *Chem. Phys. Lett.* **1991**, *187*, 143.
(26) Henderson, D.; Schmickler, W. *J. Chem. Phys.* **1985**, *82*, 2925.
(27) Amokrane, S.; Badiali, J. P. *Electrochim. Acta* **1989**, *34*, 39.
(28) Aers, G. C.; Inglesfield, J. E. *Surface Sci.* **1989**, *217*, 367.
(29) Trasatti, S. *J. Electroanal. Chem.* **1984**, *172*, 27.
(30) Ho, K. M.; Harmon, B. N.; Liu, S. H. *Phys. Rev. Lett.* **1980**, *44*, 1531. Kolb, D. M.; Boeck, W.; Ho, K. M.; Liu, S. G. *Ibid.* **1981**, *47*, 1921.
(31) Boeck, W.; Kolb, D. M. *Surf. Sci.* **1982**, *118*, 613.
(32) Otto, A. *Z. Phys.* **1968**, *216*, 398.
(33) Kretschmann, E. *Z. Phys.* **1971**, *241*, 313.
(34) Tadjeddine, A.; Kolb, D. M. *Proc. 4th Int. Conf. on Solid Surfaces*, Cannes, Vol. 1, p 615.
(35) Dhzavakhidze, P. G.; Kornyshev, A.; Tadjeddine, A.; Urbakh, M. *Phys. Rev. B* **1989**, *39*, 13106.
(36) Richmond, G. In *Electrochemical Interfaces*; Abruña, H. D., Ed.; VCH Publishers: New York, 1991.
(37) Richmond, G.; Robinson, G. M.; Shannon, V. L. *Prog. Surf. Sci.* **1988**, *28*, 1.
(38) Corn, R. M.; Higgins, D. A. *Chem. Rev.* **1994**, *94*, 107.
(39) Weber, M.; Liebsch, A. *Phys. Rev. B* **1987**, *35*, 7411; **1987**, *36*, 6411.
(40) Liebsch, A. *Phys. Rev. Lett.* **1988**, *61*, 1233. Liebsch, A.; Schaich, W. L. *Phys. Rev. B* **1989**, *40*, 5401.
(41) Guyot-Sionnest, P.; Tadjeddine, A.; Liebsch, A. *Phys. Rev. Lett.* **1990**, *64*, 1678.
(42) Leiva, E.; Schmickler, W. *Surf. Sci.* **1993**, *291*, 226.
(43) Bradley, R. A.; Georgiadis, R.; Kevan, S. D.; Richmond, G. L. *J. Chem. Phys.* **1993**, *99*, 5535.
(44) Furtak, T. E.; Simpson, L. J.; Tang, Y. *Phys. Rev. B* **1992**, *46*, 1719.
(45) Fedak, D. G.; Florio, J. V.; Robertson, W. D. In *The Structure and Chemistry of Solid Surfaces*; Somorjai, G. A., Ed.; Wiley: New York, 1969.
(46) Ertl, G. *Surf. Sci.* **1985**, *152/153*, 328.
(47) Kolb, D. M.; Dakkouri, A. S.; Batina, N. In *Nanoscale Probes of the Solid/Liquid Interface;* Gewirth, A. A., Siegenthaler, H., Eds.; NATO ASI Series; Kluwer Academic Publishers: Dordrecht, 1995.
(48) Kolb, D. M. In *Structure of Electrified Interfaces*; Lipkowski, J., Ross, P. N., Eds.; VCH Publishers: New York, 1993.
(49) Toney, M. F.; Melroy, O. R. In *Electrochemical Interfaces*; Abruña, H. D., Ed.; VCH Publishers: New York, 1991.
(50) Kolb, D. M.; Schneider, J. *Electrochim. Acta* **1986**, *31*, 929.
(51) Somorjai, G. A.; van Hove, M. A. *Progr. Surf. Sci.* **1989**, *30*, 201.
(52) Fu, C. L.; Ho, K. M. *Phys. Rev. Lett.* **1989**, *63*, 1617.
(53) Bohnen, H. P. Unpublished results, private communication.
(54) Ocko, B. M.; Helgesen, G.; Schardt, B.; Wang, J.; Hamelin, A. *Phys. Rev. Lett.* **1992**, *23*, 3350.
(55) Magnussen, O. M.; Wiechers, J.; Behm, R. J. *Surf. Sci.* **1993**, *289*, 139.
(56) Gao, X.; Hamelin, A.; Weaver, M. *Phys. Rev. B* **1991**, *44*, 10983.
(57) Flynn-Sanders, D. K. et al. *Surf. Sci.* **1991**, *253*, 2701.
(58) Häberle, P.; Fenter, P.; Gustafson, T. *Phys. Rev. B* **1989**, *39*, 5810.
(59) Moritz, W.; Wolf, D. *Surf. Sci.* **1985**, *163*, L655.
(60) Vleig, E.; Robinson, I. K.; Kern, K. *Surf. Sci.* **1990**, *233*, 248.
(61) Ashcroft, N. W.; Mermin, N. D. *Solid State Physics*; Holt: Rinehart and Winston, 1976.
(62) Lucas, J. M. S. P. *Appl. Phys.* **1965**, *36*, 1632.
(63) Greene, R. F.; O'Donnel, R. W. *Phys. Rev.* **1966**, *147*, 599.
(64) Watanabe, M. *Surf. Sci.* **1973**, *34*, 759.
(65) Rath, D. L. *J. Electroanal. Chem.* **1983**, *150*, 521.
(66) Christoph, R.; Siegenthaler, H.; Rohrer, H.; Wiese, W. *Electrochim. Acta* **1989**, *34*, 1011.
(67) Halbritter, J.; Repphuhn, G.; Vinzelberg, S.; Staikov, G.; Lorenz, W. *Electrochim. Acta* **1995**, *40*, 1385.
(68) Pan, J.; Jing, T. W.; Lindsay, S. *J. Phys. Chem.* **1994**, *98*, 4205.
(69) Vaught, A.; Jing, T. W.; Lindsay, S. M. *Chem. Phys. Lett.* **1995**, *236*, 306.
(70) Kolb, D. Private communication.
(71) Schmickler, W.; Henderson, D. J. *J. Electroanal. Chem.* **1990**, *290*, 283.
(72) Pleskov, Yu. V.; Rotenberg, Z. A. In *Advances in Electrochemistry and Electrochemical Engineering*; Gerischer, H., Tobias, C. W., Eds.; Wiley: New York, 1978.
(73) Sebastian, K. L.; Doyen, G. *Surf. Sci.* **1993**, *290*, L703; *J. Chem. Phys.* **1993**, *99*, 6677.
(74) Rostkier-Edelstein, D.; Urbakh, M.; Nitzan, A. *J. Chem. Phys.* **1994**, *101*, 8224.
(75) Sass, J. K.; Gimzewski, J. K. *J. Electroanal. Chem.* **1991**, *308*, 333.
(76) Repphuhn, G.; Halbritter, J. *J. Vac. Sci. Technol.* **1995**, *A13*, 1963.
(77) Schmickler, W. *Surf. Sci.* **1995**, *335*, 416.
(78) Mosyak, A.; Nitzan, A.; Kosloff, R. *J. Chem. Phys.* **1996**, *104*, 1549.
(79) Stillinger, F. H.; Rahman, A. *J. Chem. Phys.* **1978**, *68*, 666.
(80) Barnett, R. N.; Landmann, U.; Cleveland, C. L.; Jortner, J. *J. Chem. Phys.* **1988**, *88*, 4429.

(81) Nitzan, A. Lecture presented at the 46th meeting of the International Society for Electrochemistry, Xiamen, 1995, and private communication.
(82) Lindsay, S. M.; Jing, T. W.; Pan, J.; Lamper, D.; Vaught, A.; Lewis, J. P.; Sankey, O. F. In *Nanoscale Probes of the Solid/Liquid Interface*; Gewirth, A. A., Siegenthaler, H., Eds.; NATO ASI Series 288; Kluwer: Dordrecht, 1995.
(83) Marcus, R. A. *J. Chem. Phys.* **1965**, *24*, 966.
(84) Miller, R. J. D.; McLendon, G. L.; Nozik, A. J.; Schmickler, W.; Willig, F. *Surface Electron Transfer Processes*; VCH Publishers: New York, 1995.
(85) Smith, B. B.; Hynes, J. T. *J. Chem. Phys.* **1993**, *99*, 6517.
(86) Iwasita, T.; Schmickler, W.; Schultze, J. W. *Ber. Bunsenges. Phys. Chem.* **1985**, *89*, 138; *J. Electroanal. Chem.* **1985**, *194*, 355.
(87) Dogonadze, R. R. In *Reactions of Molecules at Electrodes*; Hush, N. S., Ed.; Wiley: New York, 1971.
(88) Kornyshev, A. A.; Kuznetsov, A. M.; Ulstrup, J. *J. Phys. Chem.* **1994**, *98*, 3832.
(89) Koene, L.; Sluyters, J. H.; Sluyters-Rehbach, M. *J. Electroanal. Chem.* **1996**, *402*, 57.
(90) Diesing, D.; Lohrenegel, M.; Otto, A. *Ber. Bunsenges. Phys. Chem.* **1995**, *99*, 1402.
(91) Carnie, S. L.; Chan, D. Y. C. *J. Chem. Phys.* **1980**, *73*, 2949.
(92) Blum, L; Henderson, D. *J. Chem. Phys.* **1981**, *74*, 1902.
(93) Blum, L.; Henderson, D.; Parsons, R. *J. Electroanal. Chem.* **1984**, *161*, 389.
(94) Badiali, J. P.; Goodisman, J.; Rosinberg, M. *J. Electroanal.* **1983**, *143*, 73.
(95) Badiali, J. P.; Rosinberg, M.; Vericat, F.; Blum, L. *J. Electroanal. Chem.* **1983**, *158*, 253.
(96) Schmickler, W.; Henderson, D. *J. Chem. Phys.* **1984**, *80*, 3381.
(97) Schmickler, W.; Henderson, D. *J. Chem. Phys.* **1986**, *85*, 1650.
(98) Schmickler, W.; Henderson, D. *Phys. Rev. B* **1984**, *30*, 802.
(99) Leiva, E.; Schmickler, W. *J. Electroanal. Chem.* **1986**, *205*, 323.
(100) Henderson, D.; Schmickler, W. *J. Chem. Phys.* **1986**, *82*, 2925.
(101) Price. D.; Halley, W. *J. Electroanal. Chem.* **1983**, *150*, 347.
(102) Kornyshev, A. A. *Electrochim. Acta* **1989** 1829. Feldman, V. I.; Kornyshev, A. A.; Partenskii, M. B. *Solid State Commun.* **1985**, *53*, 157.
(103) Amokrane, S.; Russier, V.; Badiali, J. P. *Surf. Sci.* **1989**, *217*, 425.
(104) Halley, J. W.; Johnson, B.; Price, D.; Schwalm, M. *Phys. Rev. B* **1985**, *31*, 7695. Halley, J. W.; Price, D. *Phys. Rev. B* **1988**, *38*, 9357.
(105) Amokrane, S.; Badiali, J. P. *Electrochim. Acta* **1989**, *34*, 39; *J. Electroanal. Chem.* **1989**, *150*, 315. Amokrane, S. Thesis, Paris, 1989.
(106) Duh, D. M.; Perera, D. M.; Haymet, A. D. J. *J. Chem. Phys.* **1995**, *102*, 3736.
(107) Vossen, M.; Forstmann, F. *J. Chem. Phys.* **1994**, *101*, 2379.
(108) Spohr, E. *Chem. Phys. Lett.* **1993**, *207*, 214.
(109) Glosli, J.; Philpott, M. *J. Chem. Phys.* **1992**, *96*, 6962.
(110) Patey, X. Talk presented at the meeeting of the American Chemical Society in Honolulu, Dec 1995.
(111) Schmickler, W.; Henderson, D.; Melroy, O. *Chem. Phys. Lett.* **1993**, *216*, 424.
(112) Price, D. L.; Halley, J. W. *J. Chem. Phys.* **1995**, *102*, 6603.
(113) Grahame, D. C. *Chem. Rev.* **1947**, *41*, 441.
(114) Lipkowsky, J.; Stolberg, L. In *Adsorption of Molecules at Electrodes*; Lipkowski, J., Ross, P. N., Eds.; VCH: New York, 1992.

CR940408C